

A high-resolution modelling study of the Turkish Straits System

Gianmaria Sannino¹ · Adil Sözer^{2,3} · Emin Özsoy^{2,4} 

Received: 3 November 2015 / Accepted: 8 February 2017 / Published online: 20 March 2017
© Springer-Verlag Berlin Heidelberg 2017

Abstract High-resolution modelling, for the first time, is used to study the basic hydrodynamics of the Turkish Straits System (TSS). Hydraulic controls in the Bosphorus and Dardanelles Straits are found to be essential in determining the coupled response of the TSS, which directly influences the interaction between the Mediterranean and Black Seas. The mixed baroclinic—barotropic response of the system is investigated as a function of the net barotropic flux and density stratification imposed at external boundaries, in the absence of atmospheric and tidal effects. The intense surface jet issuing from the Bosphorus is found to drive the basin-wide circulation of the Marmara Sea, varying with the net flux. The temporal response of the Bosphorus and Dardanelles Straits picks up rather fast, within a day or two, thanks to hydraulic controls within straits, while the surface currents in the Marmara Sea only approach steady state after a few months. Model stratification and circulation features are validated against independent measurements and a stand-alone model of the Bosphorus.

Keywords Bosphorus · Dardanelles · Marmara Sea · Turkish Straits System · Hydrodynamics · Model

1 Introduction

The Turkish Straits System (Fig. 1a) consists of the Sea of Marmara (surface area 11,500 km²) connected with the Aegean and Black Seas, respectively through the Dardanelles (length 75 km, min. width 1.3 km) and Bosphorus (length 35 km, min. width 0.7 km) Straits. The Marmara Sea has three elongated depressions (max. depth 1350 m) interconnected by sills (depth ~600 m) and adjoining continental shelves. The two straits, Bosphorus and Dardanelles, are shallow waterways of complex topography.

The Dardanelles (Fig. 1b) extends in a northeast orientation from the Aegean Sea and makes two strong right angle turns at Nara Pass (26° 22.5' E), where it is also the narrowest. A deep channel of 75 m depth runs through the Strait and later turns east (26° 45' E) in the southern part of the funnel shaped area, finally joining the western depression of Marmara Sea.

The Bosphorus (Fig. 1c) southern end is funnel shaped, with the deep channel starting from the northern shelf of the Marmara Sea rising north towards the entrance, passing the junction with the Golden Horn Estuary (41° 01.5' N) and meeting with the complex southern sill of 30 m depth flanked by deeper channels of 40 m on its two sides (41° 02' N). The deep channel then meets the contraction (41° 04.5' N), the narrowest section and also the deepest point (110 m) in the Strait, where the channel makes some right angle turns. From here towards north, the channel first has a straight section, then swings first to the northeast, then to northwest and once more to northeast, passing aside shallow banks and headlands, finally exiting to the Black Sea, where the thalweg depth is 75 m. A shallow cut canyon then extends northeast from the

This article is part of the Topical Collection on *the 47th International Liège Colloquium on Ocean Dynamics, Liège, Belgium, 4–8 May 2015*

Responsible Editor: Yajing Yan

✉ Emin Özsoy
ozsoyem@itu.edu.tr

¹ Italian National Agency for New Technologies, Energy and Sustainable Economic Development, Rome, Italy

² Institute of Marine Sciences, Middle East Technical University, Mersin, Turkey

³ Fatsa Faculty of Marine Sciences, Ordu University, Ordu, Turkey

⁴ Eurasia Institute of Earth Sciences, İstanbul Technical University, İstanbul, Turkey

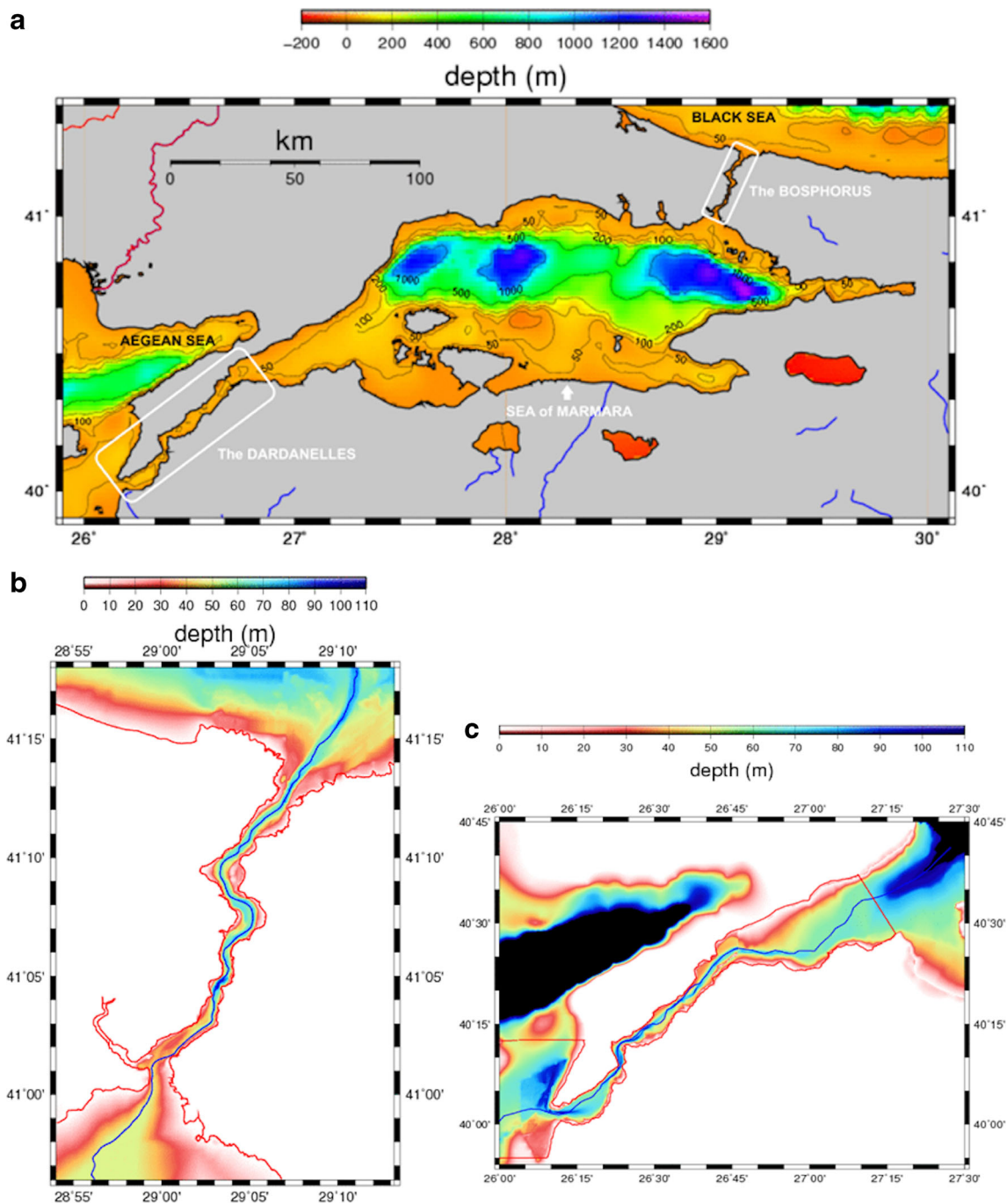


Fig. 1 Location and bottom topography maps for **a** Turkish Straits System (TSS) including **b** Dardanelles and **c** Bosphorus Straits. The blue line denotes the thalweg along the strait channels

Strait, and later swings to the northwest across the Black Sea shelf. Shortly after exit into the Black Sea, a shallow area elevated to 60 m depth inside the canyon ($41^{\circ} 16' \text{ N}$) constitutes the controlling sill depth of the Bosphorus. The thalweg in Fig. 2a runs along the deepest points, passing over the troughs and sills along the route from the Aegean Sea to the Black Sea.

The first scientific study of the Bosphorus Strait by Marsili (1681) in the seventeenth century identified the role of hydrostatic pressure difference created by the different water masses of the adjacent seas and explained the existence of a counter-current of Mediterranean water below the surface flow of Black Sea water (Defant 1961; Soffientino and Pilson 2005;

Pinardi 2009). Marsili based his conclusions on the first quantitative density measurements in history, shown to be comparable with modern day measurements (Pinardi et al. 2016), and also carried out a simple laboratory experiment to demonstrate his theory.

The northern sill outside the Bosphorus, standing at 60 m depth in the canyon cutting across the Black Sea shelf, as well as the contraction in the southern Bosphorus (Fig. 1c) are the main geometrical constrictions in the path of the flow where hydraulic controls are expected (Latif et al. 1991, Dorrell et al. 2016) and verified by model results (Sözer 2013; Sözer and Özsoy 2017) to be responsible in establishing a maximal exchange regime as predicted by Farmer and Armi (1986). A single contraction at the Nara Pass (Fig. 1b) subjects the flow in the Dardanelles Strait to sub-maximal hydraulic control (Latif et al. 1991; Ünlüata et al. 1990).

Short reviews on the TSS showing its role in coupling of the two larger Seas have been provided by Beşiktepe et al. (1993, 1994, 2000) and Schroeder et al. (2012), while other details such as its influence on the Black Sea and the Mediterranean Sea can be found in reviews by Özsoy and Ünlüata (1997, 1998) and Jordà et al. (2016). Particular information based on experimental studies of the Bosphorus Strait and its exit regions can be found in the works by Ünlüata et al. (1990), Latif et al. (1991), Özsoy et al. (1995, 1996, 1998, 2001), Gregg et al. (1999), Gregg and Özsoy (1999, 2002), Jarosz et al. (2011a,b, 2012, 2013), Book et al. (2014) and Dorrell et al. (2016). Measurements in the Bosphorus and Dardanelles Straits and their exit regions have revealed rapid currents and hydraulic controls with high shear and turbulence zones involving many different time scales of motion in the TSS, ranging from inertial, semi-diurnal, diurnal to several days periods influenced by the adjacent basins.

Climatological estimates of water fluxes based on water and salt budgets of the TSS coupled with the Black Sea have been given in Ünlüata et al. (1990), Beşiktepe et al. (1993, 1994), Tuğrul et al. (2002), as reviewed in Schroeder et al. (2012) and Jordà et al. (2016), Mavropoulou et al. (2016) and others. These computations show increased fluxes at the Dardanelles relative to the Bosphorus, and large entrainment fluxes across the halocline throughout the TSS. The annual average upper and lower layer fluxes of the Bosphorus, respectively, were estimated as 650 and 325 km³/years (20,500 and 10,300 m³/s) in the above references, in agreement with the long-term salt budget of the Black Sea requiring an approximate ratio of ~2 between the output and input mass fluxes (Özsoy and Ünlüata 1997). The mean net flux of water exiting the Black Sea is therefore estimated to be about 325 km³/years (10,300 m³/s).

Instantaneous measurements of Bosphorus fluxes from ship mounted ADCP on board the R/V BİLİM of the Institute of

Marine Sciences, METU (Özsoy et al. 1996, 1998) during the years 1991–1995 yielded statistical average fluxes of 17,000 and 3500 m³/s respectively for the upper and lower layers for the whole set of measurements, despite some data losses near the bottom and surface. The maxima of the instantaneous fluxes were about 50,000 and 20,000 m³/s, respectively, 2–3 times larger than the annual mean fluxes. These observational data are summarized and compared with model results later in Fig. 23.

Similar measurements to date seem to indicate that mean values of fluxes through the TSS are difficult to establish with certainty. This is because the mean values are actually masked by the great variability observed in the currents, indicating the experiment duration possibly being too short to establish statistics such as the mean from the variable response on daily to inter-annual time scales. For instance, mean values of the upper, lower layers and the total flux, respectively, were found to be 11,900, 8000, 3900 m³/s in the northern Bosphorus, and 14,100, 10,600, 3500 m³/s in the southern Bosphorus based on 6 months of moored instrument data obtained from the continuous measurement campaign of the NATO Undersea Research Center (NURC) starting in 2008 (Jarosz et al. 2011a, b). Based on similar but year-long data, the upper, lower layer and total (net) fluxes were 25,700, 14,000, 11,700 m³/s in the eastern (Marmara) and 36,700, 31,700, 5000 m³/s in the western (Aegean) sections of the Dardanelles Strait (Jarosz et al. 2013). These measurements confirmed the great variability in fluxes, but more importantly showed noticeable differences of the net fluxes (3900, 3500, 11,700, 5000 m³/s) between any two sections. With differences of net flux between sections obtained to be on the order of or even larger than the mean value of the net fluxes, it is very difficult to explain the disparity by sources/sinks of water between sections, as they are scarce in the region.

The average volume fluxes computed from the 10 years of monthly measurements campaign of Altıok and Kayışoğlu (2015) produced mean upper, lower layer and net fluxes of 12,800, 7900, 4900 m³/s at the northern exit of the Bosphorus Strait and 13,700, 7800, 4900 m³/s, respectively, at the southern exit of the Strait. In this case, the net flux is conserved between the two ends of the Strait, which is the expected behaviour.

Recent assessments of CTD-based hydrographic and ADCP-based flux measurements are provided by Özsoy and Altıok (2016a, b), where the results from different data sources and methodologies are compared.

Buoyant surface jets issuing at the Marmara and Aegean junctions of the two Straits, as well as bottom plumes of dense water on the other ends of the Straits transmit mass, momentum and materials from one basin to the next (Latif et al. 1991; Hüsrevoğlu 1999; Özsoy et al. 2001, Delfanti et al. 2013). The upper layer circulation in the Marmara Sea is driven by the extension of the buoyant Bosphorus surface jet, usually following an S-shaped loop between the two Straits that breaks up into smaller cells of a complex pattern in winter, subject to seasonal wind forcing. The current in the lower layer is much

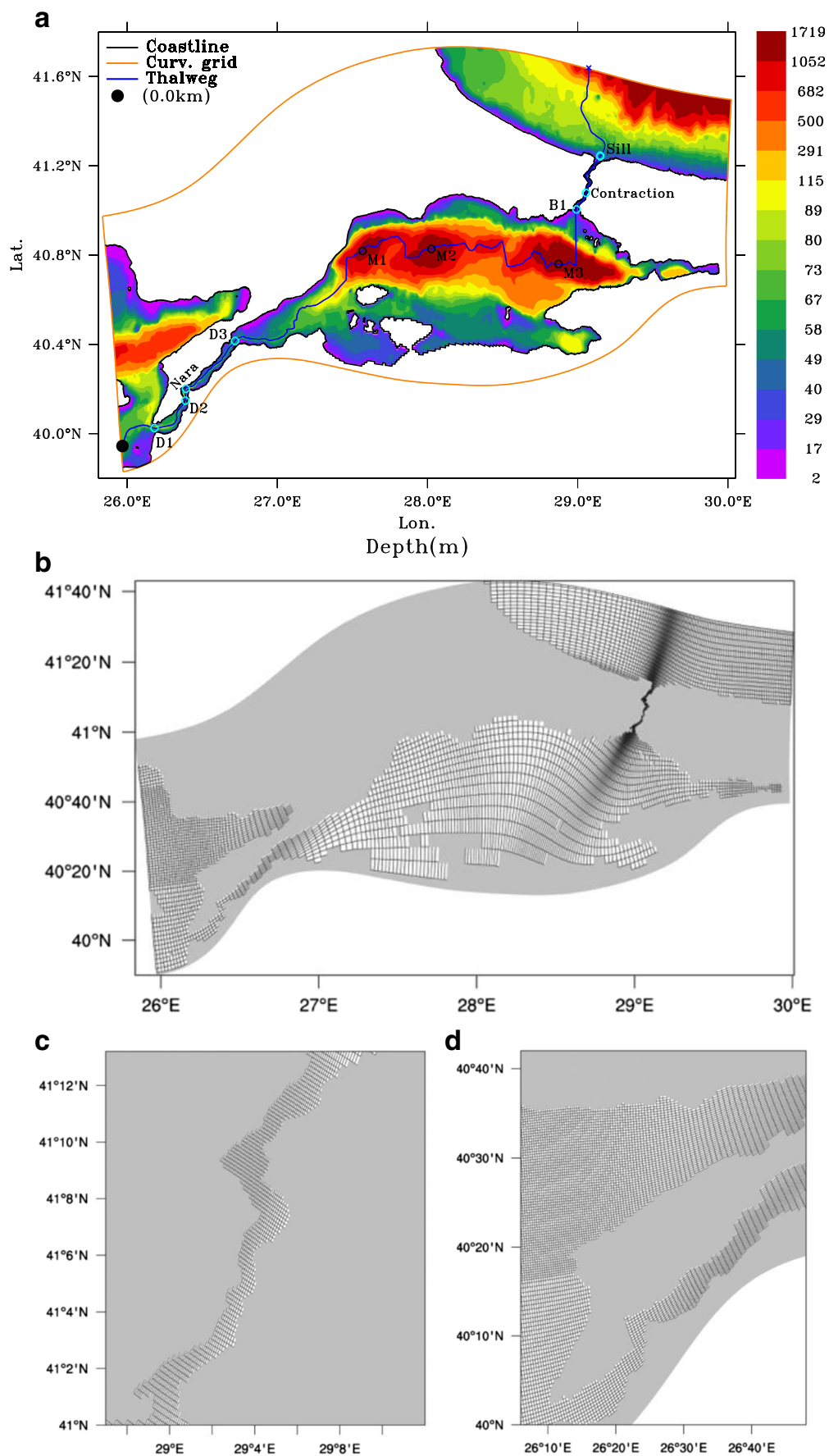


Fig. 2 **a** Model bottom topography (depth in meters), the domain limits (red line) in the adopted curvilinear coordinate system, and the thalweg (blue line) connecting the deepest points across the TSS (where the black point marks the zero point from which the distances are measured in later Figures), **b** model grid domain (for the sake of readability are shown only every 8th grid point in both directions), **c** model grid detail for the Strait of Dardanelles (every 3rd grid point), **d** model grid detail for the Strait of Bosphorus (every 3rd grid point)

weaker; it follows either the southern shelf (mostly in summer) or cascades down to fill the western basin (in some winters) depending on the incoming water density (Ünlüata et al. 1990; Beşiktepe et al. 1994).

The relatively small but significant changes in the lower layer reflect deep-water renewal processes in the Marmara Sea (Beşiktepe et al. 1993, 1994). The dense water entering via Dardanelles entrains water and sinks to the depth of equilibrium within the interior. Depending on the initial density contrast of the Dardanelles and the weak interior density stratification of the interior, the renewal process has inter-annual dependence. A reduced gravity model (Hüsrevoğlu 1999) has shown the influx to reach the bottom of the western basin in winter, later to overflow into the central basin in a time frame of few months. In summer, with a smaller density contrast, the flow is found to first proceed preferentially along the shallow depths of the southern shelf, eventually overflowing into the interior. CFC-11 below the halocline in Marmara Sea shows two maxima, one up to 300 m and the other below 700 m depth, confirming the seasonal divergence of the Dardanelles inflow either penetrating deep or staying at intermediate depth in the Marmara Sea (Beşiktepe et al. 1994). Isotope tracers oxygen-18, deuterium and tritium (Rank et al. 1998; Özsoy et al. 2002) and Cs-137 (Delfanti et al. 2013) demonstrate exchanges between the adjacent basins, as proposed by coupled box models (e.g. Maderich 1998).

From a modelling standpoint, the task of coupling adjacent basins with highly contrasting properties in a region of extreme hydro-climatic variability had to be approached in a staircase of simpler steps. The various simplified models only considering the sub-domains of the system or addressing selected processes achieved to date show the need for a sustained effort of integrated TSS modelling. Two-layer, one-dimensional or two-dimensional models solving either horizontally or vertically integrated hydrodynamic equations have been developed for the Dardanelles Strait (Oğuz and Sur 1989; Staschuk and Hutter 2001) and for the Bosphorus Strait (Oğuz et al. 1990; Ilıcak et al. 2009), capturing some basic features of the flow but often oversimplifying the topographically controlled, three-dimensional flows. Three-dimensional models solving the full set of primitive equations have been developed for the Dardanelles Strait (Kanarska and Maderich 2008) and for the Bosphorus Strait (Sözer and Özsoy 2002; Oğuz 2005; Sözer 2013; Sözer and Özsoy 2017).

As regards Bosphorus Strait, a stand-alone model of the strait developed by Sözer (2013) and Sözer and Özsoy (2017)

explained some observed features, including the blocking and hydraulic transitions of the flow (Latif et al. 1991), the sharp changes of the free surface at the contraction (Gregg and Özsoy 1999, 2002), and the separation of the zero-velocity surface with the pycnocline (Tolmazin 1985; Gregg and Özsoy 1999) also demonstrated by some of the earlier models. More importantly, Sözer and Özsoy (2017) showed hydraulic controls at anticipated locations from observational studies, providing a unique demonstration of the “maximal exchange” hypothesis applied to the hydraulic regime of the Bosphorus.

Blain et al. (2009) have used an unstructured mesh model of the Dardanelles Strait (150 m minimum cell size) in order to address the role of the Dardanelles outflow on the Aegean Sea modelled at coarser resolution. Despite their extreme variability, the exchange flows at the Dardanelles Strait are of central importance for the North Aegean Sea circulation and mixing (Androulidakis et al. 2012a, b; Tzali et al. 2010; Kokkos and Sylaios 2016; Mavropoulou et al. 2016).

The various modelling studies of the system components have still remained far from being fully representative of the coupled dynamics of the TSS in an integrated model configuration. Very few modelling studies have ever been attempted to study the TSS dynamics. Existing modelling studies have attempted to treat the Marmara Sea as an isolated marine basin, with the sole addition of inflow and outflow boundary conditions at the junctions of the Sea with the Bosphorus and Dardanelles Straits, effectively decoupling the dynamics of these straits from the basin, for instance, as reported by Demyshev and Dovgaya (2007), Demyshev et al. (2012) and Chiggiato et al. (2011).

Demyshev et al. (2012) integrated their model for up to 18 years to reach quasi-steady equilibrium state, arriving at a basic description of the circulation driven by heat, salt, and momentum exchanges through the Bosphorus and Dardanelles Straits without the effects of atmospheric forcing. According to their results, the geostrophic adjustment of currents occurred in about 50 days, whereas the spin-up including the evolution of the density field in the deep basin lasted for about 3 years. A quasi-steady feature, namely the S-shaped jet current described by Beşiktepe et al. (1994) is found to be directed from the Bosphorus Strait to the Dardanelles with maximum velocities of up to 60 cm/s. A cyclonic eddy is formed periodically near the northern boundary of the Marmara Sea with a seasonal lifetime of about 230 days as a result of jet slowing and widening in the spring and summer seasons. The same model was later run with only wind stress forcing (Demyshev, personal communication), showing the breakup of the circulation into cyclonic and anticyclonic eddies as also documented by the measurements of Beşiktepe et al. (1994). Chiggiato et al. (2011) similarly applied inflow and outflow lateral boundary conditions at the junctions of the Straits with the Sea of Marmara, and used atmospheric forcing to show the various possible patterns of

mainly wind-driven circulation superposed on the basic flow generated by flows imposed from Straits.

Recent modelling advances have attempted to achieve better horizontal and vertical resolution including details of the strait dynamics coupled with the Marmara Sea and partially representing the adjacent Aegean and Black Sea domains as areas to specify boundary conditions, with an aim eventually to couple with the models developed separately for these basins. Gündüz and Özsoy (2015) have based their model on the HYCOM (Bleck and Boudra 1981) with a grid size of 400 m, trying to achieve sufficient resolution for the Marmara Sea, although of course not sufficient at the straits, in order to compute the response to atmospheric forcing, together with whatever exchange flows that were generated in their limited area model. This effort has been partially successful, especially in correlating the macro-scale characteristics such as the effects of the outflow to the Aegean Sea, while at the Straits, precise simulation of the exchange flows could not possibly be obtained at such resolution, despite the considerable computational load required. Later, Gündüz (2016) used the same TSS model based on HYCOM, but at 4 km horizontal resolution and ten vertical levels (not resolving the straits) to compute surface trajectories under combined effects of winds and volume fluxes, which verified the existence of an S-shaped current (described also further below) carrying objects from near the Bosphorus to the Marmara Island in the southwest, typical for summer circulation, when wind-driven currents are of less consequence. On the other hand, concerning the model simulations of Chiggiato et al. (2011) under combined effects of lateral fluxes and surface forcing, it is probably no wonder that the predominantly wind-driven circulation was successfully verified against observations, despite the fact that dynamics of the Straits were not taken into account.

In direct contrast with a number of other studies lacking either the needed resolution or the coverage, and complementary to the unstructured grid modelling of Gürses et al. (2016), we presently aim for improved representation of the domain. We claim to show that the Marmara Sea hydrodynamics cannot be adequately understood or even resolved, unless substantial dynamics of the Straits are fully accounted for in the system. The nonlinear, strongly stratified hydrodynamics of the flow through the narrow Straits has made the modelling of the TSS a grand challenge, not only because of the need to adequately resolve the fine details, but also with an absolute need to account for several active processes which normally do not come into play in typical applications of open ocean or coastal models. The strategy to address these challenges, dictated by the problem itself, is to treat the entire TSS as an integral system, with a finely resolved model essentially accounting for the energetic flows with nonlinear hydraulic controls, hydraulic jumps and turbulent mixing processes in the Straits, also with an active free surface and steep topography,

within the same model. This challenge has been taken, relying on the available high-resolution topography, advanced model physics and numerical implementation, making use of the available data for initial conditions, in order to investigate basic behaviour of the system. We will try to show that this integrated approach is justified for better predictions of system behaviour.

We note however that our aim in the present study has been to investigate the behaviour of the coupled TSS model with respect to different values of a steady state net volume flux. The system, initialized with typical vertical property distributions of the adjacent basins with initial lock-exchange configuration at the two Straits is integrated until quasi-steady state is reached. Including atmospheric forcing or tidal effects was not our primary concern in this paper, since this had been done, for example in Chiggiato et al. (2011), who applied observed fluxes at Strait junctions, but did not consider coupling with the dynamics of the two Straits. In contrast, we investigate the effects of a primary (steady state or seasonal) forcing mechanism of applied net flux in the absence of unsteady forcing imposed by the atmospheric or tidal effects. The unsteady response of the TSS under additional effects due to atmospheric forcing are investigated by Gürses et al. (2016).

In Section 2 we provide details of the model, its configuration, and describe the observations used for initialization and validation. In Section 3 we interpret model results in respect to the flow structure, validating them with observations and stand-alone model results. Discussion and conclusions are given in Section 4.

2 Model configuration and setup

In this study, the Massachusetts Institute of Technology general circulation model (MITgcm, <http://mitgcm.org>) is used to study this extreme environment with full details of its contrasting properties. The MITgcm solves both the hydrostatic and non-hydrostatic Navier-Stokes equations under the Boussinesq approximation for an incompressible fluid with a spatial finite-volume discretization on a curvilinear computational grid. In this study, the hydrostatic version of the model has been implemented. The model formulation, which includes implicit free surface and partial step topography is described in detail by Marshall et al. (1997a, b). As for similar recent applications (Sanchez-Garrido et al. 2011; Naranjo et al. 2014; Sannino et al. 2014, 2015; McKiver et al. 2016) an implicit linear formulation of the free surface is used.

The high-resolution (20 m gridded) bathymetric data used for Bosphorus and Dardanelles hydrodynamics models have been kindly made available by our late colleague Erkan Gökaşan (Gökaşan et al. 2005, 2007) with the permission of

the Turkish Navy, Navigation, Hydrography and Oceanography Office. The bathymetry for the remaining part of the model domain is based on the General Bathymetric Chart of the Oceans GEBCO_08 gridded data having a resolution of 30 arc-seconds. The bathymetric data are interpolated to the model grid, and the thalweg running along the Turkish Straits System from the Aegean Sea through the Dardanelles Strait, the three deep depressions of the Marmara Sea and past the Bosphorus Strait to the Black Sea shelf edge following the narrow canyon is obtained by determining the deepest point on any cross-section along the way (Fig. 2). The very high horizontal resolution adopted in MITgcm, together with the partial cell formulation allows a very detailed description of the bathymetry.

No-slip conditions are imposed at the bottom and lateral solid boundaries. The selected tracer advection scheme is a third-order direct space-time flux limited scheme due to Hundsdorfer et al. (1995). Following the numerical experiments conducted by Sanchez-Garrido et al. (2011) and Sannino et al. (2014) to investigate the 3-D evolution of large amplitude internal waves in the Strait of Gibraltar, the turbulent closure parametrization for vertical viscosity and diffusivity proposed by Pacanowski and Philander (1981) has been used. Horizontal diffusivity coefficient is chosen as $K_h = 2 \cdot 10^{-2} \text{ m}^2 \text{ s}^{-1}$, whereas variable horizontal viscosity follows the parameterization of Leith (1968). No flux conditions for either momentum or tracers and no-slip conditions for momentum are imposed at the solid boundaries. Bottom drag is expressed as a quadratic function of the mean flow in the

bottom layer: the (dimensionless) quadratic drag coefficient is set equal to 0.02.

The model domain chosen extends over the entire TSS, including also parts of the Northeast Aegean Sea and the Black Sea at its two ends. In particular, the horizontal grid is tilted and stretched at the Bosphorus and Dardanelles Straits to better follow the main axis of the TSS. A non-uniform curvilinear orthogonal grid (1728×648 grid points) covers the domain at variable resolution, ranging from less than 50 m in the two Straits up to about 1 km in the Marmara Sea (Fig. 2). The model grid is shown in Fig. 2b for the entire domain, in Fig. 2c, d for the Dardanelles Strait and the Bosphorus Strait, respectively. We note however, that the number of nodes displayed in these Figures is much reduced in comparison to the actual grid, as indicated in the Figure label.

In order to adequately resolve the complex hydraulic dynamics of the TSS in a region of highly variable topography, the model vertical grid has been designed to have 100 vertical z -levels of inhomogeneous distribution with respect to depth. The thickness between consecutive levels is exponentially varied in the range from 1.2 m at the surface up to 110 m at the bottom, with about half of the levels concentrated in the first 100 m (Fig. 3). The remaining 50 levels cover the rest of the water column down to the maximum depth of 1730 m. This distribution of vertical levels has been selected to ensure a very good vertical representation of the two shallow Straits and without sacrificing too much the vertical discretization in the deeper Marmara Sea. Furthermore, it resolves the surface layer as well as the density interface rather well, allowing to

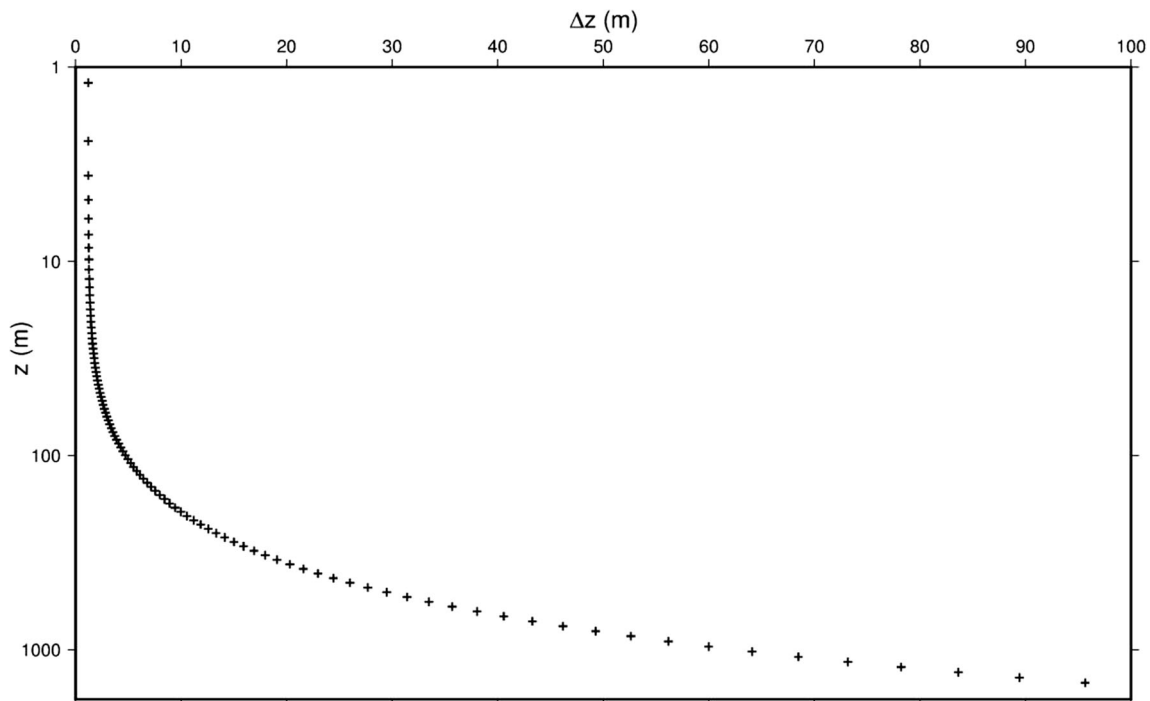


Fig. 3 Layer thickness Δz versus layer depth z (log scale) for the model vertical grid of 100 model levels

keep interfacial mixing under control. We stress that such a model grid configuration (both horizontal and vertical) represents a novelty with respect to any other ocean model implemented in the same region in the past.

We use CTD measurements to derive the initial conditions and also to verify the modelling results, based on the intensive measurements carried out in June–July 2013 in the high-energy environments of the TSS and the Black Sea continental shelf/slope region. The objective for the TSS experiment was to capture the post-spring stratified conditions on the shelf and slope regions, in the narrow Straits and channels and their deeper neighbourhood, and specifically to investigate the intrusive effects of the Mediterranean effluent in the adjacent Black Sea. Observational data on physical and chemical variables in the region have been collected on board the R/V BİLİM during 18 June–06 July 2013. The bathymetry of the region and the stations occupied by the R/V BİLİM cruise are shown in Fig. 4.

The model is initialized with three different water masses filling the western part of the domain, the Marmara Sea and the eastern side of the domain, respectively, with vertical profiles selected from CTD casts (Fig. 5) obtained during the cruise of the R/V BİLİM of the Institute of Marine Sciences in June–July 2013 (Fig. 4). The only available concurrent profile in the shallow region near the Aegean Sea exit of the Dardanelles Strait has been extended to the bottom, considering the relatively small changes in properties in the deeper parts of the Aegean Sea

proper, that only influence the lower layer over longer than annual time scales. With the initial condition specified as only vertical variations in the three basins and lock exchange at the two straits, the model is left free to adjust to steady state by two-way exchange through the system.

At the northern and western open boundaries, a 3D relaxation of salinity and temperature towards the initial condition data was applied, with the relaxation time varying from 3 to 30 days over the first 30 grid points. Therefore, the model grid covering the Aegean Sea and Black Sea work as restoring boxes that force the baroclinic exchange of water masses through the Dardanelles and Bosphorus. This consolidated modelling approach has been extensively used over the last 20 years to simulate the water exchange between Atlantic Ocean and Mediterranean Sea (Roussenov et al. 1995; Demirov and Pinardi 2002; Tonani et al. 2008; Carillo et al. 2012; Sannino et al. 2015).

The model is forced through the specification of the same barotropic flux (but opposite sign) at both ends of the model domain. The barotropic flux is applied in the form of surface fresh water input that is constrained to change only the volumes of the Black Sea and Aegean Sea boxes.

In order to highlight the effects of different barotropic net flux values on the resulting circulation in the Marmara Sea and in the two Straits, other external forcing components were deliberately left out as steady state solutions to barotropic forcing were sought. In other words, the model does not include atmospheric

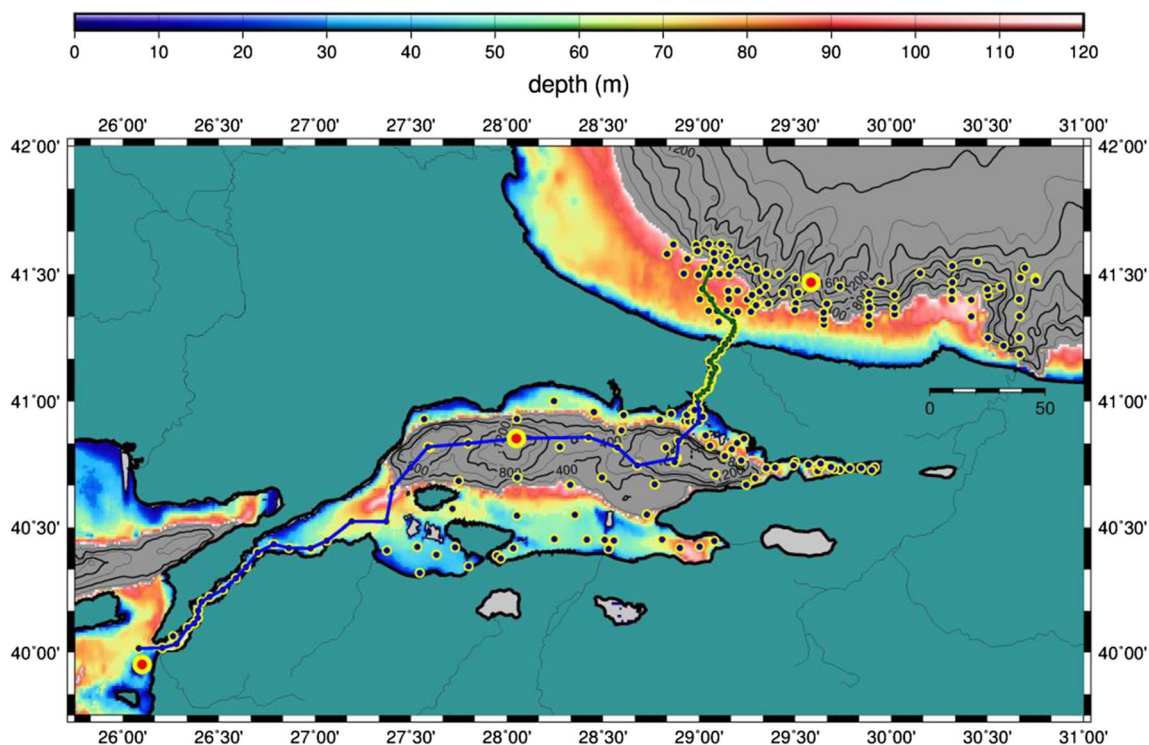


Fig. 4 Locations of CTD sampling stations (black dots) during the June 18–July 06, 2013 cruise of the R/V BİLİM, with the selected CTD stations (red dots) at coordinates (41°28'N 29°35'E), (40°51'N 28°03'E) and (39°57'N 26°06'E), respectively to represent the Aegean Sea,

Marmara Sea and the Black Sea. Bathymetry of the shelf regions up to 200 m depth are shown with the colour scale, and depths greater are shown with contours of 200 m interval. The blue and green lines correspond to vertical transects of properties displayed later

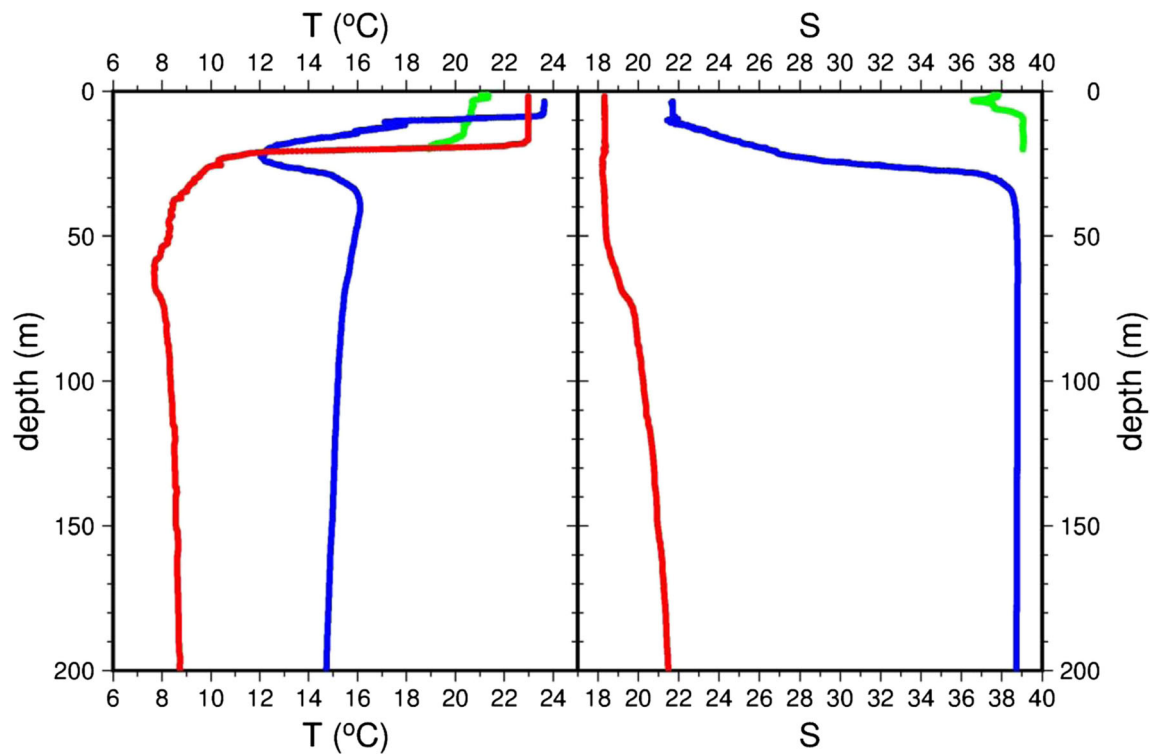


Fig. 5 Temperature and salinity profiles selected to represent initial conditions in the Black Sea (*red*), Marmara Sea (*blue*) and Aegean Sea (*green*) domains of the model, respectively, corresponding to the three CTD stations shown in Fig. 4 (*red dots*)

forcing at the surface and any tidal signals applied on any open boundaries.

3 Results

3.1 Flow characteristics

3.1.1 Basic set of experiments performed

The response of the currents and density structure over the water column to different net flow is examined through a basic setup of experiments with varying net barotropic volume flux values. The model in each case has been initialized with selected CTD profiles (June–July 2013) representative of the three basins, as described above.

A modest comment on the total duration of the model runs is in order here. Firstly, as model runs were planned to optimize computational cost, aiming to achieve absolute steady state would prove to be prohibitive. Equilibrium in this system actually would not be easy to define in a strict sense, as the TSS is a coupler as well as a buffer for conditions in adjacent basins. Tracers could not be used to establish steady-state, as the estimates for mean residence time extend from a few months at the surface layer to 6–7 years in the deeper waters (Beşiktepe et al. 1994) to 12–32 years

(Lee et al. 2002, at 100–450 m depths of the eastern basin, based on CFC tracer ages). Therefore, one should primarily aim for steady-like behaviour at the surface layer. Furthermore, the necessarily restricted geometry of the adjacent basins in the model meant that absolute equilibrium solutions were not possible and in fact were not aimed. All of the runs therefore did not have the same length, although they were sufficiently long to reach quasi-steady state, beyond which the TSS circulation did not seem to undergo much of a qualitative change. Most runs were verified to have reached a reasonable steady state in about 2 months, evaluated on the criteria of net flux and kinetic energy evolution, as will be shown later. However, we present results on day 65, when we discuss features of the circulation, in order to have a common time reference for all cases.

The results from these experiments, to be described in the following, appear to capture the fine scales within the two Straits and also the meso-scale in the Marmara Sea, thanks to the non-uniform grid and the vertical resolution of the model. The results also appear satisfactory, realistically representing the structure of the interface (or the zone of maximum vertical gradient separating the upper and lower layers of relatively uniform properties), without creating excessive mixing that could otherwise destroy the initially observed sharp stratification.

3.1.2 Response to changes in net volume flux

The model experiments were performed with varying net flux values of $Q = -9600, 0, 5600, 9600, 18,000$ and $50,000 \text{ m}^3/\text{s}$, respectively. Positive values of Q represent flow from the Black Sea towards the Mediterranean, while negative values represent net flow in the opposite direction. The selected wide range of net fluxes actually corresponds to values observed during numerous measurements in the Bosphorus (e.g. Özsoy et al. 1998 and others; for a summary of past measurements of layer and net fluxes, see Fig. 23 later in the text).

The free surface variations in the Marmara Sea under varying net barotropic flux values are shown in Fig. 6, with the surface current vectors superimposed. For the studied flows driven solely by the net flux, an S-shaped current first moving south from the Bosphorus, later turning northwest and finally exiting from the Dardanelles Strait appears to be the basic character of the circulation, with one or more basin scale gyres appearing in between (Fig. 6).

With a negative flux of $Q = -9600 \text{ m}^3/\text{s}$, i.e. net flow towards the Black Sea, the upper layer flow from the Bosphorus into the Marmara Sea is still positive, and sufficient to generate an anti-cyclonic net circulation in the midst of the Marmara Sea (Fig. 6a). In this case the weak jet issuing from the Bosphorus mouth tends to attach to the western coast instead of shooting straight to the south as in the other cases with positive net flux.

For zero net flux ($Q = 0$), similar structure is preserved (Fig. 6b), but the surface currents of the jet issuing from the Bosphorus (the “Bosphorus Jet” hereafter) are already stronger than the negative net flux case, with the jet flow shooting straight out and impinging on the Bozburun peninsula on the south side of the Marmara Sea, from whence the flow bends west to join the central anticyclonic gyre. As the barotropic flux is increased further to positive values, first to $5600 \text{ m}^3/\text{s}$ and later to $9600 \text{ m}^3/\text{s}$ (Fig. 6c, d), the central gyre takes a smaller and elongated form increasingly more attached to the northern coast of the Marmara Sea, while the Bosphorus Jet bends towards the west without first touching the Bozburun Peninsula. For moderate net flows, a few small cyclonic

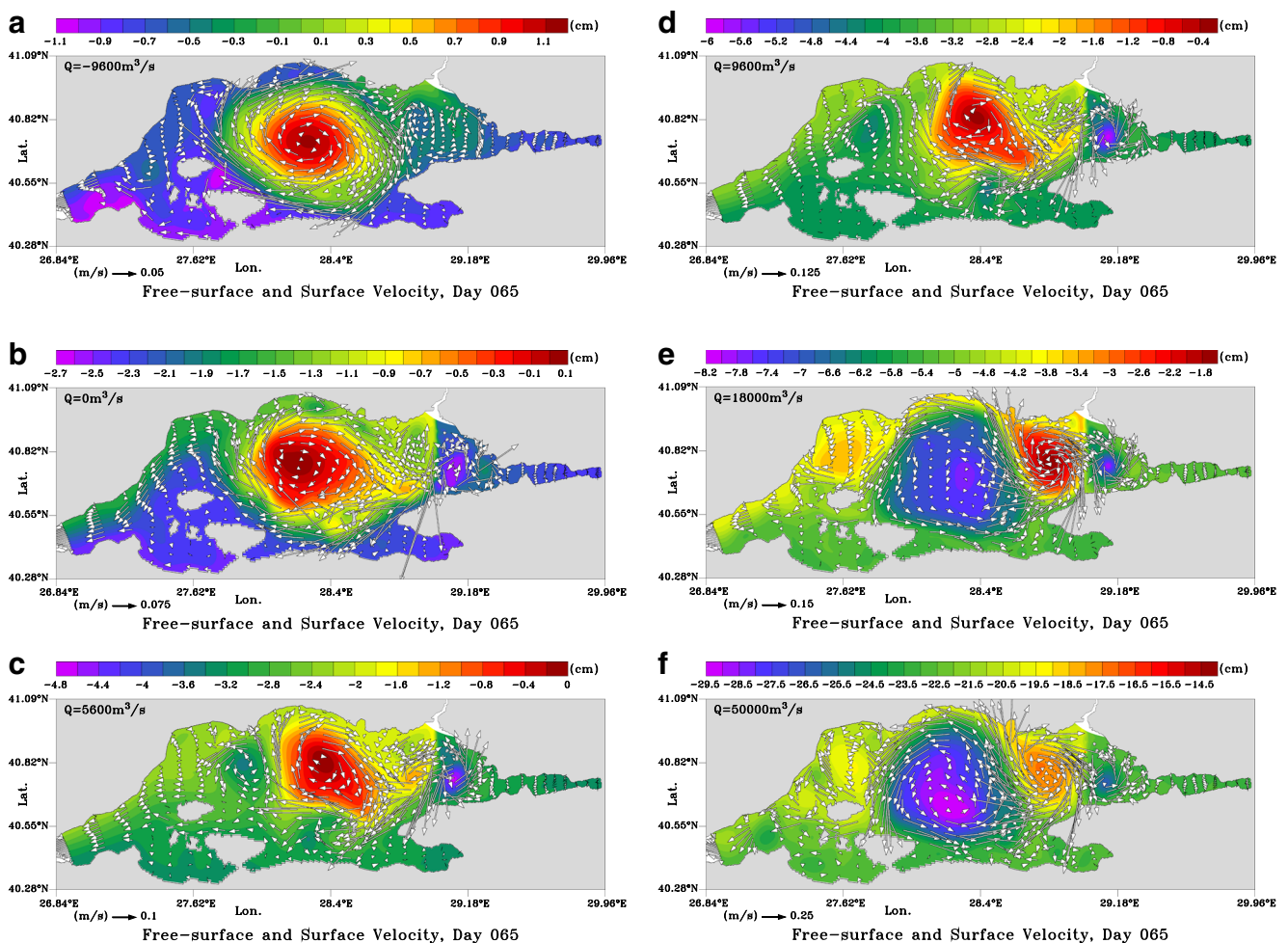


Fig. 6 a–f The free surface variations with superimposed surface currents in the Marmara Sea for varying net barotropic volume flux values of $Q = -9600, 0, 5600, 9600, 18,000$ and $50,000 \text{ m}^3/\text{s}$. The final quasi-steady solutions reached on day 65 are shown (large current vectors near Bosphorus have been masked)

eddies can be identified to the west and south of the central gyre and in the confines of the eastern basin on the eastern side of the jet.

For the extreme flux values of $Q = 18,000 \text{ m}^3/\text{s}$ and $Q = 50,000 \text{ m}^3/\text{s}$ (Fig. 6e, f), the lower layer flow in the Bosphorus becomes blocked (vertical sections for the latter case shown later in Figs. 7b and 8d), and in consequence, qualitative changes occur in the circulation of the Marmara Sea. First, the anticyclone recedes nearer to the Bosphorus exit and is unified with the jet, with a mid-Marmara cyclonic gyre occupying roughly the same location as the former central anticyclonic gyre, and a secondary anticyclone further west. In the case with the largest flux (Fig. 6f) the central cyclonic gyre strengthens further while the near Bosphorus eastern and the western anticyclonic circulation cells seem to weaken.

For all these cases, the circulation pattern looks more like the buoyancy driven flow along the coast adjacent to the mouth of a river, which in fact is the buoyant outflow of the Bosphorus jet in this case. This southward surface jet is clearly identified in cases with positive net volume flux, extending straight out from the Bosphorus and bending towards west to contribute to the anticyclonic gyre.

The generation of a basic anticyclonic circulation in the Marmara Sea for lower net fluxes, evolving towards a more balanced circulation of cyclonic-anticyclonic eddies appears to be a result of the vorticity balance of the basin. As shown by Spall and Price (1998) and studied by Morrison (2011), the net basin circulation is sensitively determined by the potential vorticity (PV) imports and exports of the basin. We can simply infer this by considering the approximate conservation of $PV = (\zeta + f)/h$ applied to the upper layer, where ζ is the relative vorticity of the upper layer current, f the Coriolis parameter (planetary vorticity) and h the thickness of the upper layer. A one-layer fluid entering from a strait to a wider region with depth change has been shown to imply changes in vorticity by Nof (1978a), who later has extended the analysis to two-layer fluids (Nof, 1978b). From this point of view, the reduction of the interface depth (or upper layer thickness) h from the Black Sea to the Marmara Sea, as required by the salt-wedge type of flow structure in the Bosphorus Strait (described later in Section 3.1.3, Figs. 7 and 8) implies a net decrease in relative vorticity ζ of the water column, with possible negative vorticity export into the Marmara Sea, which would result in the generation of an anticyclonic surface circulation upon exit to the Marmara Sea, assuming the input from the Black Sea initially to have zero vorticity. Later, in the discussion relating to Fig. 15c in Section 3.1.5, we shall provide limited evidence of the asymmetric Bosphorus Jet velocity profile, a possible indicator of the vorticity export.

The behaviour of the buoyant plume entering the Marmara Sea, initially shooting south and hitting the opposite coast is displayed in all cases in Fig. 6, although the later turning of the flow to the west is typical of buoyant plumes at this scale.

Buoyant flows entering the sea are typically attached to the right-hand-side coast (looking out from the exit in the northern hemisphere, especially if the initial vorticity is zero or below a critical limit (e.g. Nof 1978b; Stern et al. 1982). A bulge of the buoyant fluid is formed after exit, as the flow turns right to follow the coast, as often observed at river mouths (e.g. Huq 2013).

In a two-layer system with variable bottom topography and dynamically active layers, the circulation may develop differently from a topographically steered single layer flow, with topography influencing the lower layer flow, and the resultant interface topography in turn influencing the upper layer flow (Beardsley and Hart 1978). As the net flux is increased in Fig. 6, the changes in the circulation pattern may be a result of this kind of interactive adjustment of the flow layers to bottom and interface topography.

In the case of a negative net flux (i.e. towards the Black Sea, Fig. 6a), the buoyant surface jet almost ceases to exist, with the jet becoming immediately attached to the western coast. In other cases of Fig. 6 with positive fluxes, the jet shoots straight to the south, later to join the anticyclonic circulation.

The qualitative change in the circulation towards a series of anticyclonic and cyclonic eddies following the meander of the currents, when the flux is increased to 18,000 and 50,000 m^3/s is reminiscent of the Alboran Sea, where similar gyres filling the basin develop under high fluxes (Spall and Price 1998; Preller 1986; Riha and Peliz 2013).

3.1.3 Structure of flow through the TSS

The salinity cross-sections throughout the TSS are shown in Fig. 7, following the thalweg line of Fig. 2a, for selected net barotropic flux values. The upper layer thickness remains less than 25 m for fluxes up to 9600 m^3/s , and starts to increase afterwards, abruptly reaching 35 m when the Bosphorus is flushed out at the maximum flux value of 50,000 m^3/s . In the first case of $-9600 \text{ m}^3/\text{s}$ net flux towards the Black Sea, the two-layer stratification extends from the Black Sea to the Aegean Sea through the Straits, while in the latter case of an extreme net discharge of 50,000 m^3/s originating from the Black Sea, the saline lower layer has been pushed so far as the southern section of the Bosphorus and arrested there in the form of a salt wedge. The upper layer reflects modified Black Sea characteristics while the lower layer reflects Mediterranean characteristics all along the transects, while the most rapid changes in salinity occur in the Bosphorus and Dardanelles straits, by mixing between the two water masses, as also indicated by observations (Beşiktepe et al. 1993). The interface depth also varies strongly in the two straits, where fast exchange currents occur subject to hydraulic controls in the transition areas (Gregg et al. 1999; Gregg and Özsoy 1999, 2002; Özsoy et al. 2001; Ilıcak et al. 2009; Sözer 2013; Sözer and Özsoy 2017).

The expanded views of salinity cross-sections for the Bosphorus and Dardanelles are respectively shown in Figs. 8

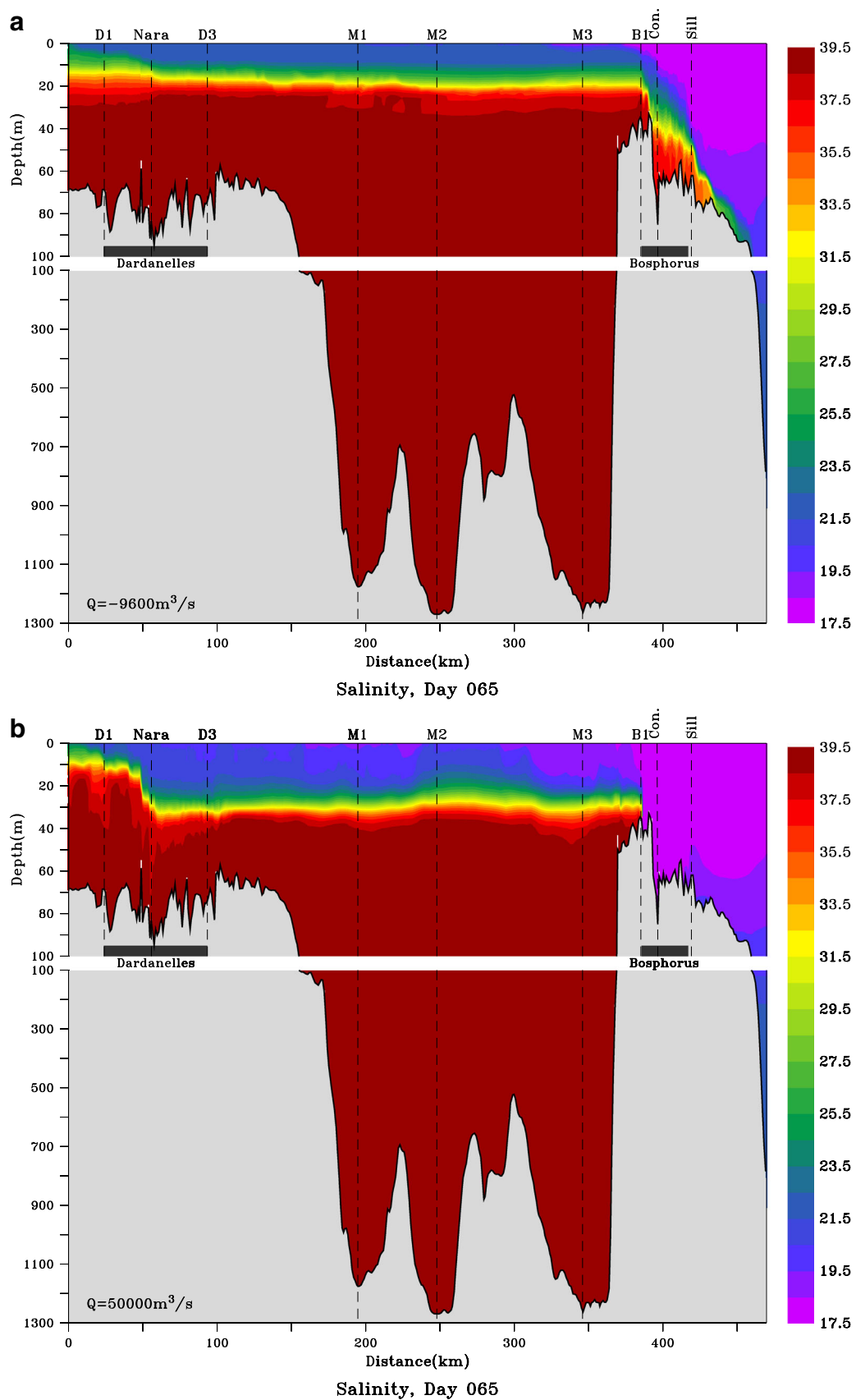


Fig. 7 Salinity cross-sections through the TSS, following the thalweg line of Fig. 2a, for selected net barotropic volume flux values of **a** $Q = -9600$ and **b** $50,000 \text{ m}^3/\text{s}$

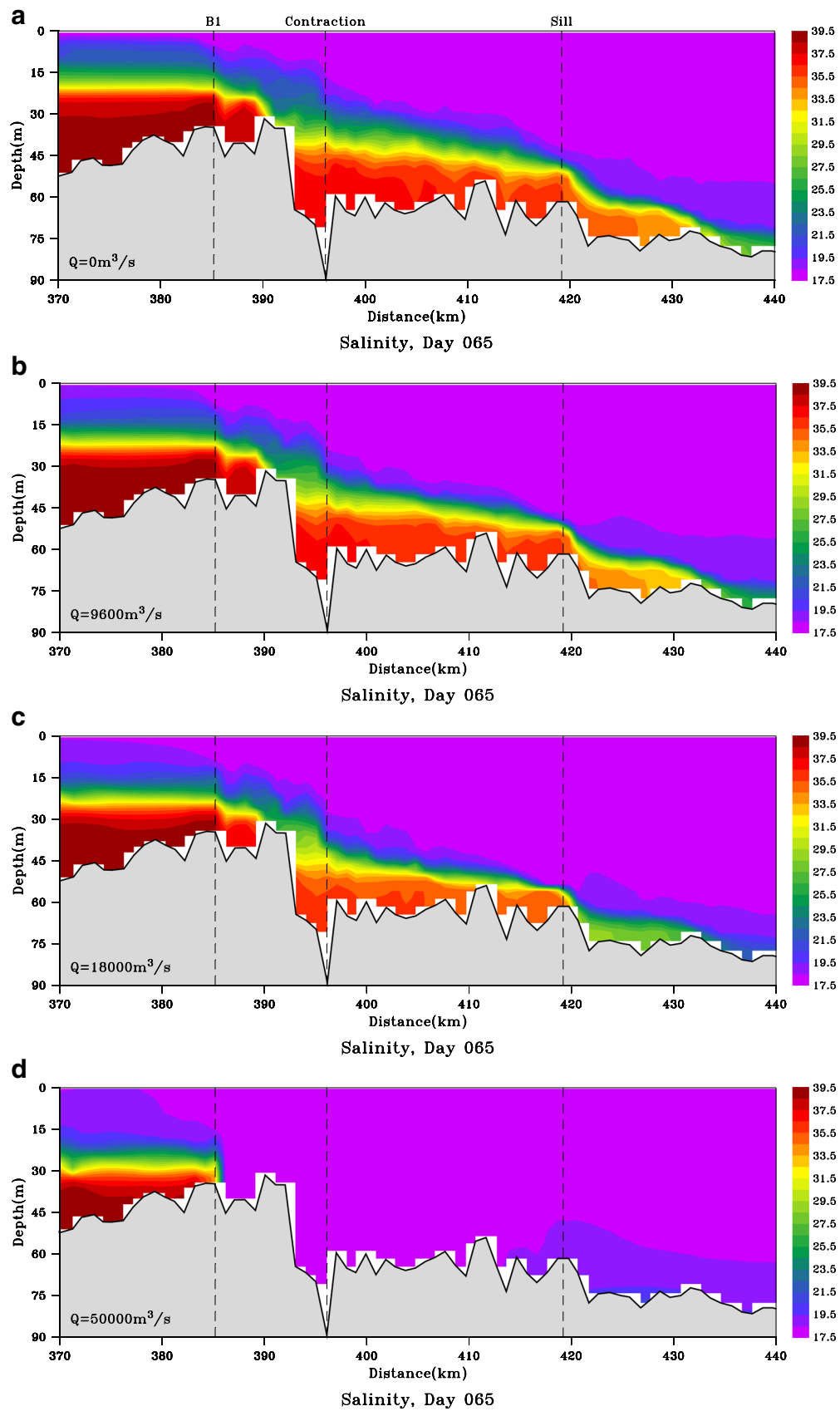


Fig. 8 Bosphorus salinity cross-sections along the thalweg in Fig. 2a, for varying net barotropic volume flux values of **a** 0, **b** 9600, **c** 18,000 and **d** 50,000 m^3/s

and 9. These cross-sections confirm the possibility of hydraulic transitions at the anticipated control sections based on past experience, better identified by higher resolution observations (Gregg et al. 1999; Gregg and Özsoy 1999, 2002; Özsoy et al. 2001) as well as in local models of the straits (İlıcak et al. 2009; Sözer 2013; Sözer and Özsoy 2017). The exact confirmation of hydraulic controls, either from observations or model results however, requires more careful analysis that often fails to show critical combined densimetric Froude numbers to be reached, unless either the complex geometry or approximations which are of higher order than the two-layer one are used, as testified by the above references.

With increasing values of net barotropic flow from zero (Fig. 8a) to intermediate values such as $9600 \text{ m}^3/\text{s}$ (Fig. 8b) the flow in the Bosphorus shows rather stable characteristics due to the existence of hydraulic controls at two critical sections, i.e. the narrows in the southern part where the channel is also the deepest, and the northern sill, in a configuration typical of the ‘maximal exchange’ regime of Farmer and Armi (1986) and verified in the Bosphorus by 3D numerical model experiments of Sözer (2013). In dissipative regions past the contraction in the south of the Strait and also north of the northern sill, the interface layer becomes thicker and the dilution effects become stronger by increased mixing.

Note however, that the mixing characteristics change first slowly and then rather abruptly when the net flux is increased past the threshold of blocking. The results do not differ much between the two cases of Fig. 8a, b, by varying the net flux from 0 to $9600 \text{ m}^3/\text{s}$, except for slight deepening of the interface and the dilution in lower layer salinity throughout the strait and rapid changes past the northern sill, where the lower layer flow undergoes a hydraulic jump entering the canyon leading up to the shelf edge northwest from the Bosphorus (Fig. 1). With further increase of the net flux to $Q = 18,000 \text{ m}^3/\text{s}$ (Fig. 8c), the lower layer becomes almost blocked at the northern sill, with only a very diluted, thin layer of saline water leaking into the Black Sea. When the flux is increased further to $Q = 50,000 \text{ m}^3/\text{s}$ (Fig. 8d) the lower layer is completely blocked and pushed back all the way to the southern Bosphorus, and even past the contraction, where it is arrested in the form of a salt wedge at the southern end of the Bosphorus. Under such extreme conditions, almost the entire Bosphorus is flushed out by water entering from the Black Sea.

Similarly, the changes in the two-layer flows in the Dardanelles Strait for the net barotropic flux values of $Q = 0$, 9600 and $50,000 \text{ m}^3/\text{s}$ are shown in Fig. 9a–c. Here the only hydraulic control exists at the narrows of the Nara Passage, where the interface undergoes rapid changes in depth. In the western part of the strait past the hydraulic transition at Nara Pass, the thickness of the interface becomes larger and the oscillations in the iso-lines testify to increased dissipation and mixing,

which may be characterizing hydraulic jumps. As the net flux is increased at first from $Q = 0$ (Fig. 9a) to $9600 \text{ m}^3/\text{s}$ (Fig. 9b), the depth of the interface on the Marmara side increases slightly, remaining around 20–25 m on the Marmara side, while drastic changes occur as the extreme flux value of $Q = 50,000 \text{ m}^3/\text{s}$ is reached (Fig. 8d), when the Bosphorus is almost totally flushed out (Fig. 9c) and as a result, the interface depth in the Marmara Sea increases abruptly to 35 m.

Note also that the sharp stratification observed in the cases of lower net flux values, which becomes weaker as the flux is increased, due to mixing generated upstream of the Dardanelles Strait and along the rest of the TSS. For increasing values of net flux, and especially for the extreme case in Fig. 9c, it can be observed that the interfacial mixing, as well as the mixing due to the dissipative hydraulic jump past the narrows becomes more significant. On the other hand, it can be noted that blocking of the Dardanelles lower layer is not achieved even with the largest value of net flux tested; this may be a consequence of the existence of a single hydraulic control anticipated in the Dardanelles Strait (sub-maximal exchange of Farmer and Armi 1986), as well as the interface depth upstream of it in the Marmara Sea, which in turn is established primarily by the Bosphorus controls.

In the absence of atmospheric and tidal forcing, the response of the Dardanelles flow appears to depend primarily on the depth of the interface and stratification in the upstream Marmara Sea, which in turn depend on the net flux and the response of the Bosphorus and Marmara Sea, while the Aegean Sea water properties influence primarily the lower layer inflow into the Marmara Sea and entrainment processes in the Strait.

3.1.4 Hydraulic controls

In the above description, the basic functional patterns of a strait such as the Bosphorus do not appear too different between the coupled TSS and the stand-alone strait models, and in fact reproduce many features documented by observations, despite the great difference in horizontal and vertical grid resolution and physical parametrizations employed by the different models. In this respect, we can speculate that the hydraulic controls, as key processes in the straits, set the scene for the basic behaviour common to both model configurations. To evaluate this dynamical reasoning, we propose to check existence of hydraulic controls inside Bosphorus Strait of the TSS model and later compare results with the higher resolution model results obtained by Sözer and Özsoy (2017) in the stand-alone case.

In order to perform analyses of hydraulic criticality of the flow in the Bosphorus Strait, we use the three-layer formulation of

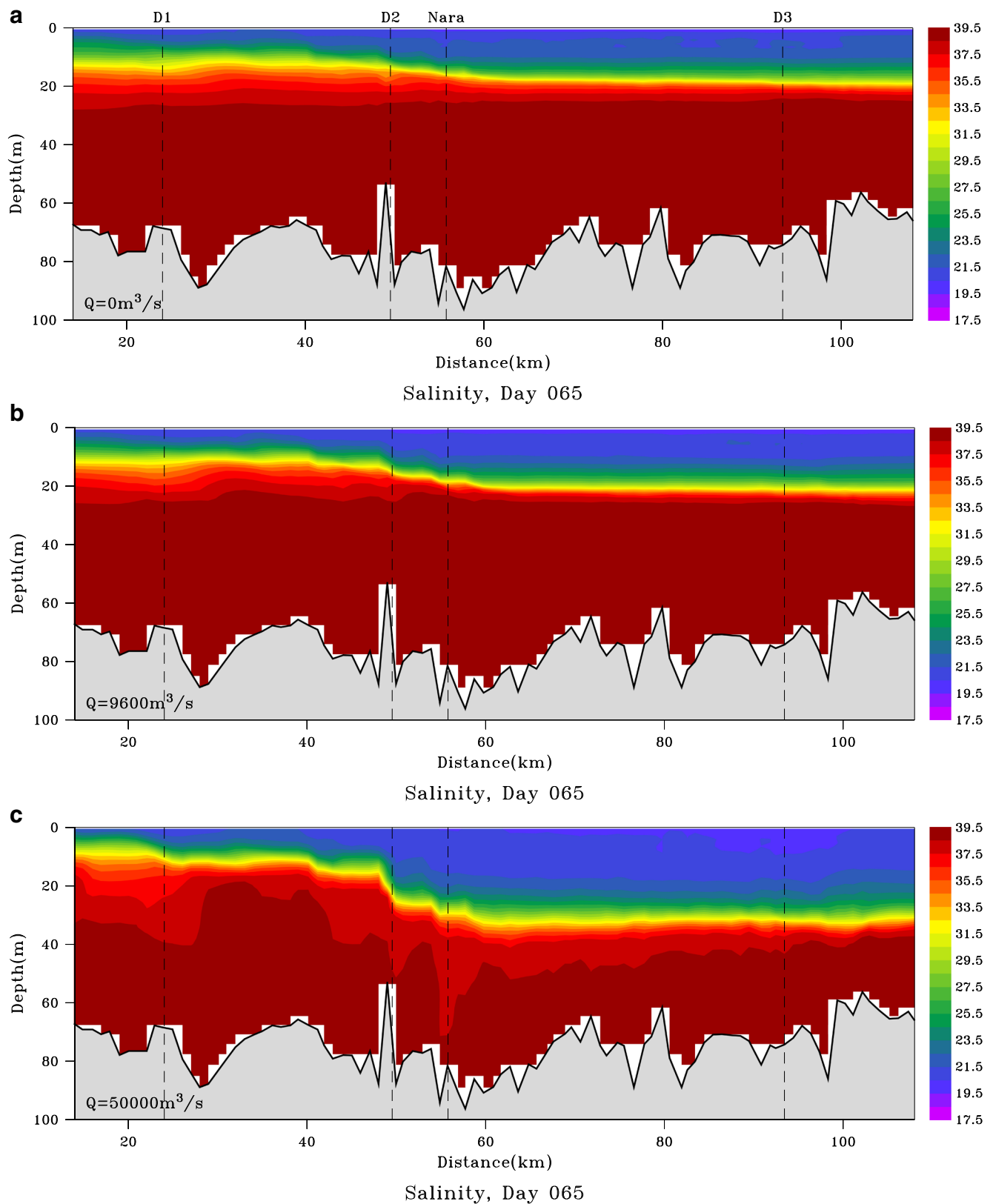


Fig. 9 Salinity cross-sections through the Dardanelles along the thalweg of Fig. 2a, for varying net barotropic volume flux values of **a** 0, **b** 9600 and **c** 50,000 m^3/s

Pratt (2008) and Sannino et al. (2009). Composite densimetric Froude number G^2 and layer Froude numbers F_i^2 for layers $i = 1-3$ have been calculated based on formulations involving transverse velocity variations after Pratt (2008) and Sannino et al. (2009, following their Eq. 3), namely

$$G^2 = F_1^2 + \left(\frac{1-r}{r} + \frac{w_3}{w_2} \right) F_2^2 + F_3^2 - \frac{w_3}{w_2} F_1^2 F_2^2 - F_1^2 F_3^2 - \frac{1-r}{r} F_2^2 F_3^2$$

where

$$F_1^2 = \left(\frac{1}{w_2} \int_{y_{1L}}^{y_{1R}} \frac{g'_{21} H_1}{u_1^2} dy_1 \right)^{-1}$$

$$F_2^2 = \left(\frac{1}{w_2} \int_{y_{2L}}^{y_{2R}} \frac{g'_{32} H_2}{u_2^2} dy_2 \right)^{-1}$$

$$F_3^2 = \left(\frac{1}{w_3} \int_{y_{3L}}^{y_{3R}} \frac{g'_{32} H_3}{u_3^2} dy_3 \right)^{-1}$$

$$g'_{32} = g(\rho_3 - \rho_2) / \bar{\rho}$$

$$g'_{21} = g(\rho_2 - \rho_1) / \bar{\rho}$$

$$r = (\rho_2 - \rho_1) / (\rho_3 - \rho_1)$$

and u_i are layer velocities, ρ_i are the layer densities, H_i and w_i are the layer depths and widths at interface for the three layers $i = 1-3$, integrated from one bank at y_{iL} to the other at y_{iR} . First a three-layer decomposition of the Bosphorus flow is achieved by defining an interfacial layer with limits assigned to 10% of the surface to bottom salinity difference, computed along the Bosphorus thalweg. The Froude numbers are then calculated by integration across the main core of the flow. Near the Marmara exit, where the flow becomes asymmetric across the wide strait, integration is carried out to within 2500 m width placed around the thalweg to make sure the active core of the surface flow is captured.

The three-layer densimetric Froude numbers calculated along the Bosphorus are presented in Fig. 10a, b. It is clear from these figures that the upper layer becomes supercritical ($F_1^2 > 1$) immediately south of the contraction with a reformation over the southern sill, followed later by the Marmara Sea exit, while the lower layer becomes supercritical past the northern sill ($F_2^2 > 1$), as has been anticipated from observations. In Fig. 10b, the modal decomposition of the layer contributions to criticality are analysed based on the criteria of Sannino et al. (2009, specified by their Eqs. 5–7). Although the existing states in the three-layer system are expected to be one of the following: (i) both modes supercritical, (ii) one of the

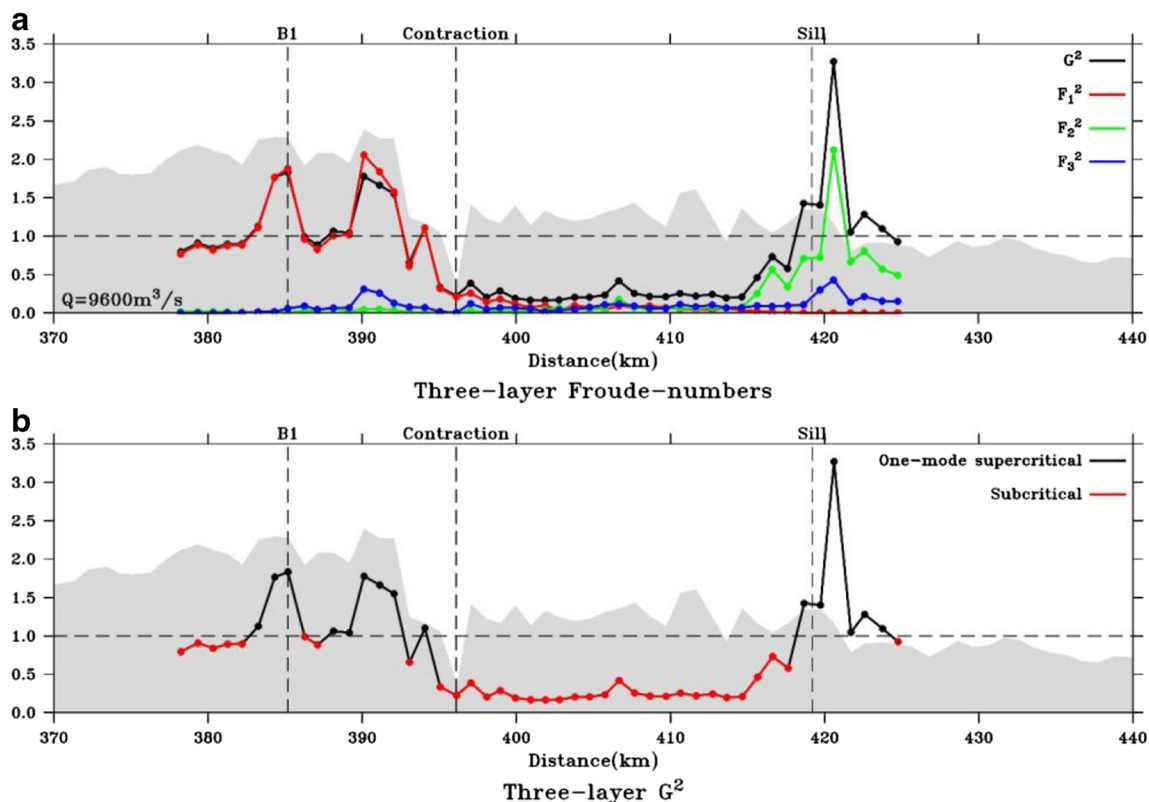


Fig. 10 Hydraulic criticality analysis based on three-layer decomposition of flow variables along the Bosphorus: **a** the three-layer composite densimetric Froude number G^2 and its components F_i^2 for layers $i = 1-$

3, b the contributions of strait modes to G^2 , indicating either only one-mode is supercritical (*black line*) as in the present case, or all modes are supercritical, according to criteria developed in Sannino et al. (2009)

modes supercritical while the other mode is subcritical or (iii) both modes subcritical, according to Sannino et al. (2009), our analyses for the case of Bosphorus only indicated single mode supercriticality in the supercritical segments (contraction-sill-exit) of the southern part of the strait and past the northern sill in the Black Sea exit region. The region between the contraction and the northern sill is in a subcritical state according to the same criteria.

The only comparisons we could make of the results with the existing literature in respect to hydraulic controls are in reference to the results of the 1D, two-layer model of Oğuz et al. (1990) and the model of Oğuz (2005) utilizing the

Princeton Ocean Model (POM) at low resolution and simplified geometry of the Bosphorus, as well as the recent 3D model results of Sözer and Özsoy (2017) described above. The Oğuz et al. (1990) model predicted hydraulic controls at the northern sill and the southern exit, but found only conditional cases of critical two-layer Froude number at the contraction, depending on the applied barotropic flux and friction. Because it was not possible to show two-layer Froude number criticality in the simplified model of Oğuz (2005), only Richardson number criticality was shown in the shear regions past the northern sill and in a wide region south of the contraction.

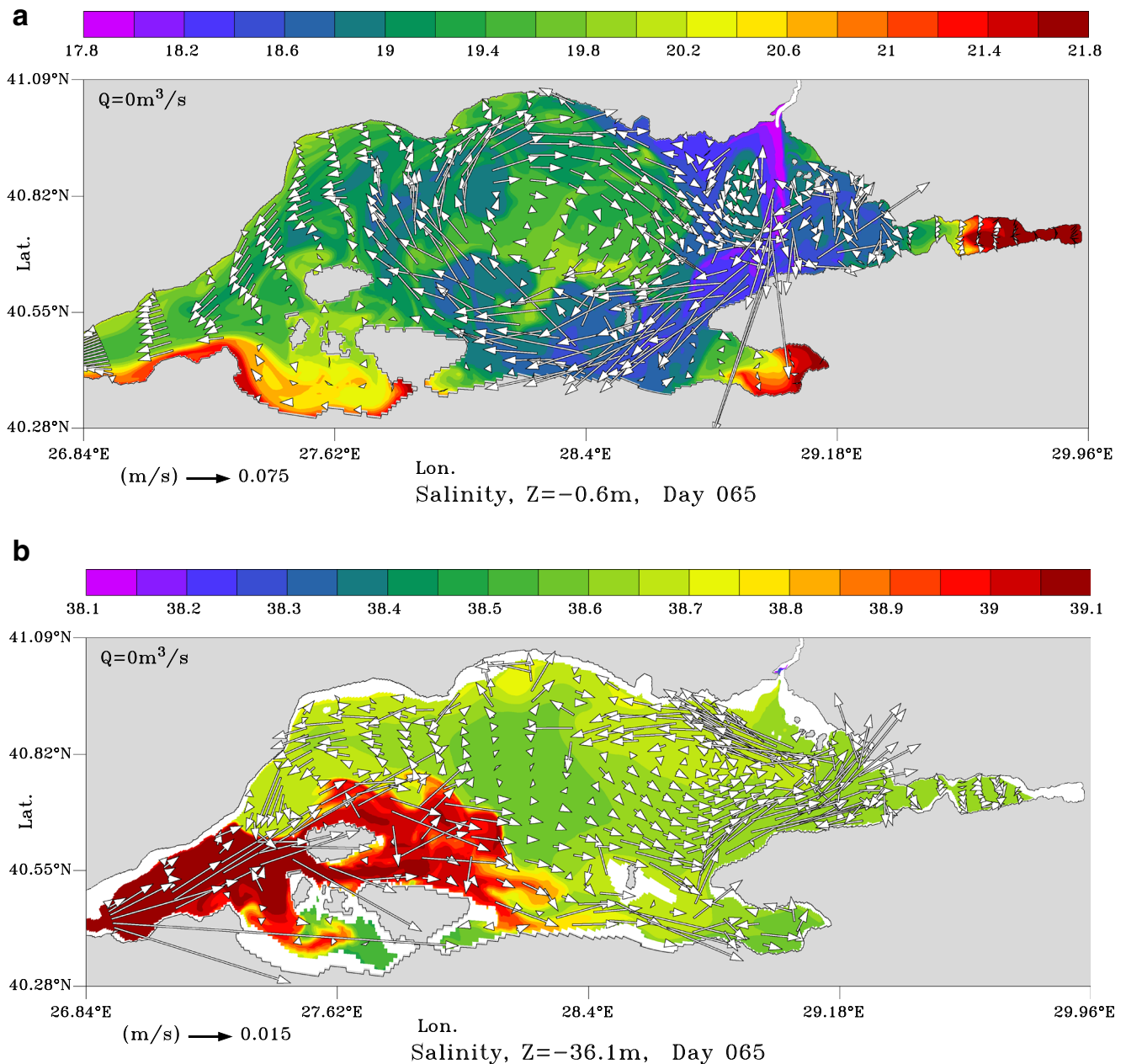


Fig. 11 Salinity and current vectors at depths of **a** 0 m (surface) and **b** 36 m in the Marmara Sea for a net barotropic volume flux of $Q = 0\text{ m}^3/\text{s}$ (large current vectors near Bosphorus have been masked)

The original analyses of hydraulic controls using both the two and three-layer approximations were originally performed for the stand-alone model of the Bosphorus (Sözer and Özsoy 2017). The two-layer Froude number calculation based on the idealized geometry Bosphorus model was able to show criticality at the northern sill, but could not show its existence at the contraction, despite the different methods of layer separation and shear corrections used. In the realistic Bosphorus case, hydraulic controls with critical transitions were found in the 2-layer approximation only after extensive shear

corrections and exclusion of shallow banks with low currents. Results of the three-layer criticality analyses based on the stand-alone Bosphorus model were actually quite similar to those obtained from the present TSS model, with almost coinciding supercritical and subcritical zones, except for a very short span along the strait where two-mode supercriticality was detected in the contraction and northern sill regions in the stand-alone case. We note that the criticality analysis depends on model resolution to allow for adequate representation of strait modes.

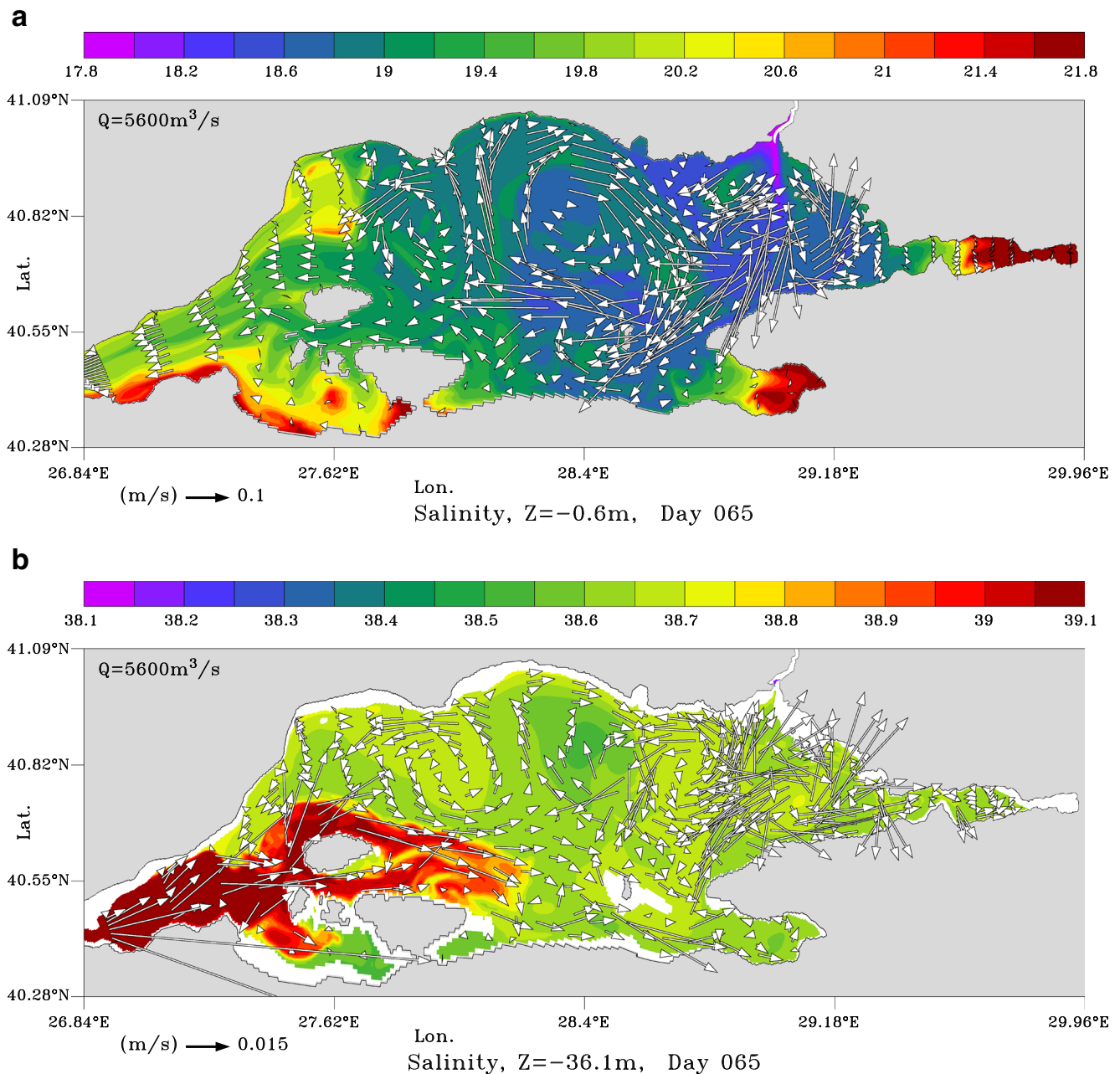


Fig. 12 Salinity and current vectors at depths of **a** 0 m (surface) and **b** 36 m in the Marmara Sea for varying net barotropic volume flux value of $Q = 5600 \text{ m}^3/\text{s}$ (large current vectors near Bosphorus have been masked)

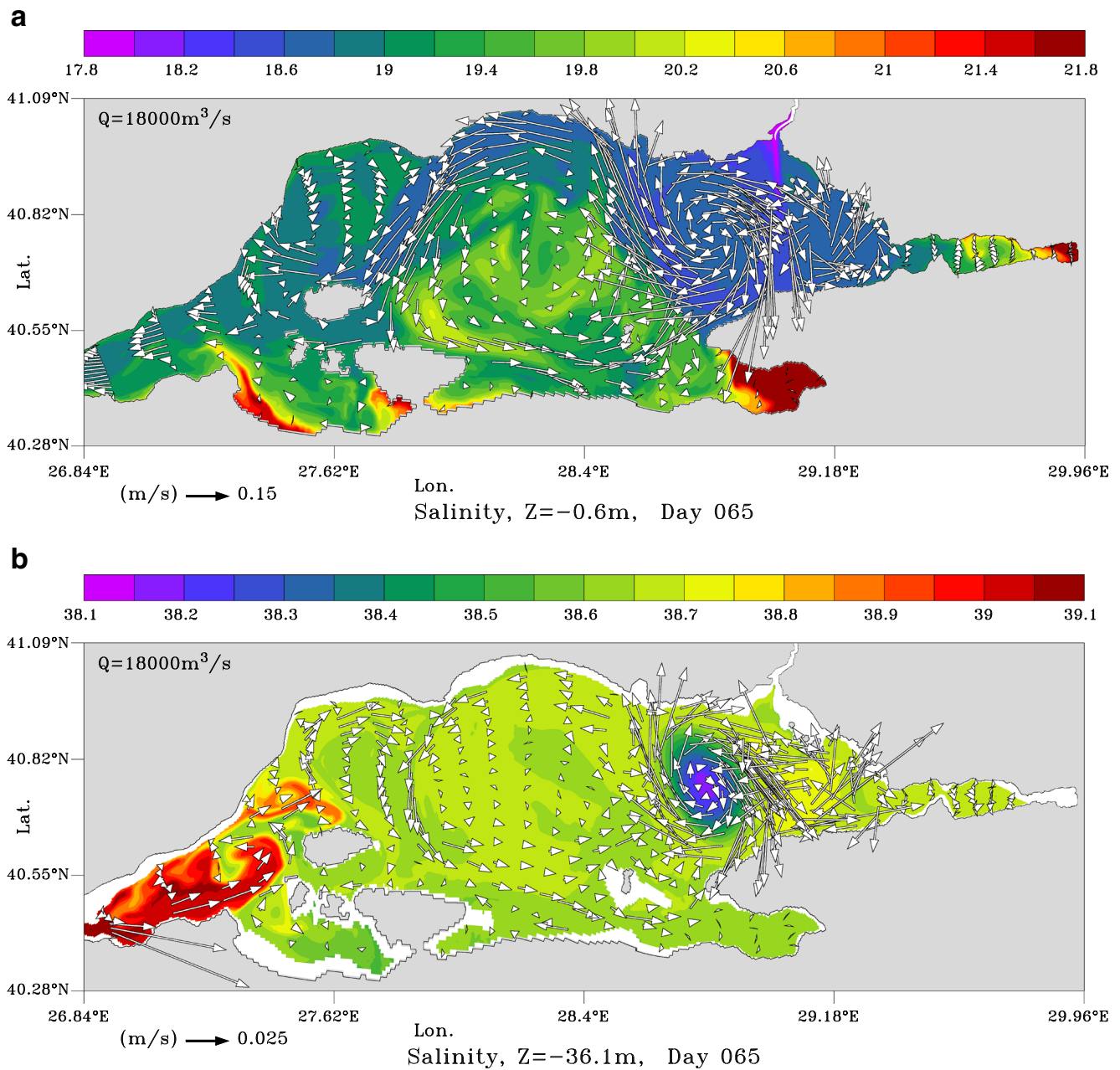


Fig. 13 Salinity and current vectors at depths of **a** 0 m (surface) and **b** 36 m in the Marmara Sea for varying net barotropic volume flux value of $Q = 18,000\text{ m}^3/\text{s}$ (large current vectors near Bosphorus have been masked)

Analyses based on the present three-layer criteria showing hydraulic transitions of the flow near essential topographic/geometric constrictions, also anticipated from earlier observations (e.g. Özsoy et al. 2001; Gregg and Özsoy 2002) and shown in the stand-alone Bosphorus model of Sözer and Özsoy (2017) provide strong support for the hypothesised “maximal exchange” regime of the Bosphorus, which has been anticipated since the early observations (e.g. Ünlüata et al. 1990; Latif et al. 1991) of the Bosphorus currents and hydrography based on the Farmer and Armi (1986) analyses of the hypothetical case.

3.1.5 The upper and lower layer circulations

The salinity and horizontal current vectors at the surface and at a depth of 36 m are shown in Figs. 11, 12, 13 for variable barotropic flows. The surface features in Figs. 11, 12, 13 reflect patterns similar to the sea level variations in Fig. 6. As the net flux is increased, the surface circulation cells become smaller but more numerous, fitting together with the meanders of the jet traversing across the basin. In the lower layer (36 m), the penetration of Mediterranean water from the Dardanelles

Strait into the Marmara Sea decreases as the net flux is increased.

We note the initial development of the Bosphorus Jet in Figs. 11, 12, 13 are indicated by its temperature and salinity anomaly rather than the current vectors; otherwise very large current vectors with magnitudes of >1 m/s result in the immediate neighbourhood of the Bosphorus, which have been masked to have better manageable graphics.

For lower values of net flux, the penetrating Dardanelles flow along the southern coast forces a reverse circulation at 36 m, which marginally represents upper part of the lower layer flows just below the interface at about 25 m. For small values of the barotropic flux (Figs. 11 and 12) the lower layer circulation is roughly cyclonic, excluding the regions affected by the Bosphorus jet, with easterly flow along the southern coast and westerly flow along the northern coast, i.e. opposite to the central anticyclonic cell in the upper layer.

A further general feature that can be noted in Figs. 11, 12, 13 is the increase in surface salinity as the net flux is increased. This may seem contrary to the increased influence of the Black Sea waters flooding the upper layer of the Marmara Sea, but on the other hand it gives rise to increased mixing and entrainment into the surface layer from the lower layer, which gives rise to higher salinities. In other words, the stronger jet influences the vertical mixing within the upper layer, in addition to the horizontal mixing induced.

As the flux is increased to $Q = 18,000$ m³/s (Fig. 13), the lower layer flow in the Bosphorus gets nearer to being blocked, and with further increase to $Q = 50,000$ m³/s it is completely blocked (as explained earlier in Figs. 7 and 8). For these extreme values of net flux, a qualitatively different circulation is developed in the Marmara Sea (Fig. 6), as the interface in the Marmara Sea deepens respectively to about 30 and 35 m (see Figs. 7, 8). The displayed salinity and currents at 36 m for the extreme flux case in Fig. 13b therefore can no longer be qualified as lower layer—these waters now become influenced to move in the same general direction with the upper layer currents.

A further feature worth mentioning in Figs. 11, 12, 13 is the relative isolation of the numerous bays (Erdek, Bandırma and İzmit Bays), where additional increases in surface salinity are consistently observed, as currents tend to bypass the relatively inaccessible interior parts of these coastal embayments.

Below the sharp pycnocline of the Marmara Sea, properties are rather uniform in Figs. 11, 12, 13 (see also the vertical sections in Figs. 7 and 8), except very near the interface where an injection of more saline water from the Dardanelles spreads below the halocline (as shown in Fig. 14 in the following), or when a strong near-surface circulation feature causes vertical displacements at this level. The spread below the halocline is typical for the summer season as shown by earlier studies (Beşiktepe et al. 1993,

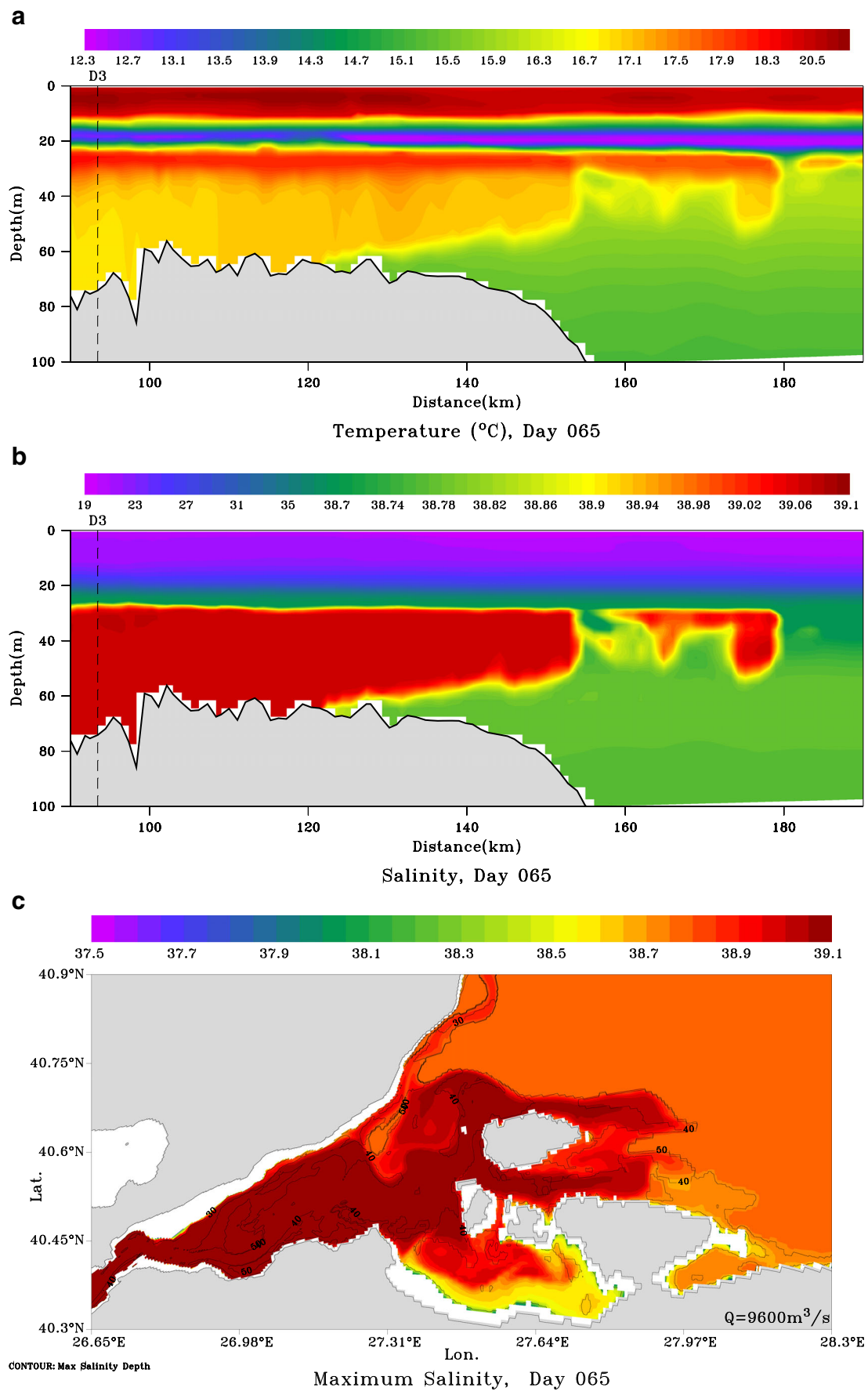
Fig. 14 Vertical sections of **a** temperature and **b** salinity near the entrance to the Marmara Sea from the Dardanelles Strait along the thalweg of Fig. 2a, **c** horizontal view of the maximum value of salinity (colour) in the vertical and depth of maximum (contours), **b** calculated near the Dardanelles Strait entrance of the Marmara Sea, for the net flux value of 9600 m³/s

1994; Hüsrevoğlu 1999), considering the June 2013 period for which the model has been initialized.

The spreading of warm and saline, dense water from the Dardanelles Strait into the Marmara Sea is visualized in Fig. 14a–c for the net flux value of 9600 m³/s. The dense water of Mediterranean origin entering the Marmara Sea from the lower layer of the Dardanelles Strait is cooler (except for a thin layer of cold water remaining from winter in the lower part of the upper layer) and more saline than the upper layer waters. On the other hand, the entering lower layer water is warmer, more saline and lighter than the interior sub-halocline waters, so that the intrusion of these waters into the Marmara Sea is clearly trapped below the halocline level, as indicated by the temperature and salinity sections in Fig. 14a, b. The maximum salinity in the vertical and the depth of this maximum in Fig. 14c shows that the inflowing water separates from the bottom, to reach equilibrium levels below the halocline, later proceeding between the island of Marmara and Kapıdağ Peninsula along the shallow southern shelf of the Marmara Sea, where it gets mixed and diluted by eddying motions on its path. This pattern is typical of the summer conditions with which the model is initialized.

The salinity distribution and current vectors at depths of 0 m (surface) and 36 m in the Bosphorus are shown in Fig. 15a–c. The surface flow (Fig. 15a) is channelled from the Black Sea into the straight northward section of the Strait, from whence it follows the sharp right angle turns of the channel with some directional overshoots. The currents at 36 m depth in the lower layer of the southern Bosphorus initially transport Mediterranean water through a narrow channel bypassing the southern sill. On approach towards the contraction, the currents speed up as the lower layer dives deeper under the southerly flowing upper layer water of Black Sea origin (shown on the same depth horizon) north of the contraction (Fig. 15b).

At the narrowest reach of the channel the upper layer flow speeds up, with a decrease in the upper layer depth, at the same time going through the anticipated hydraulic control past the contraction (Fig. 15a), and later runs parallel to the channel in the southern part. In the last reaches of the channel turning southwest before the exit (Fig. 15c), the currents lean on the Anatolian (eastern) side, trapping a weak recirculation zone on the European side of the strait (Beşiktaş) separated by the protrusion of the Sarayburnu (Seraglio) headland on the European side (north of the Golden Horn Estuary), which leads to a non-uniform profile of surface currents across the section before arriving at the Bosphorus mouth. These



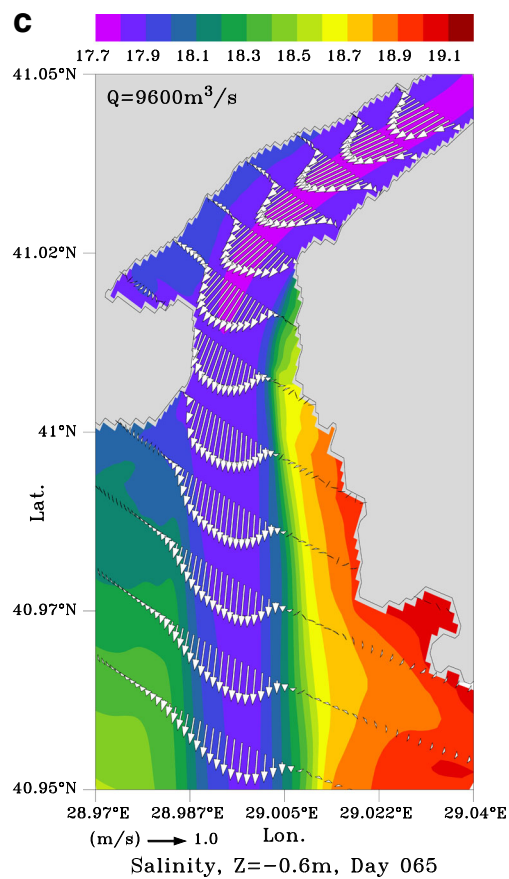
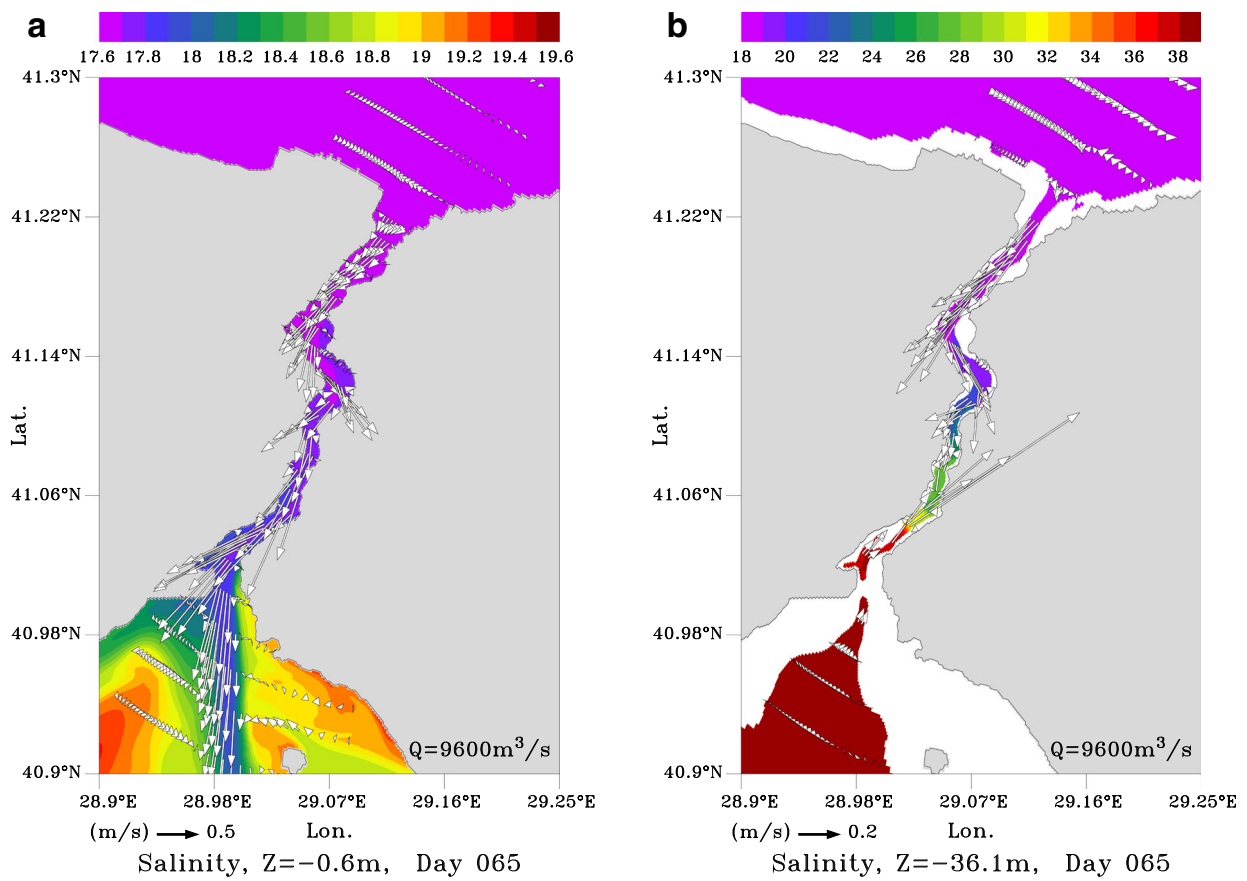


Fig. 15 Salinity and current vectors at depths of **a** 0 m (surface) and **b** 36 m in the Bosphorus, **c** with enlarged view of the surface features (vectors plotted at every 2nd grid point in east-west orientation and every 7th grid point in north-south orientation along curvilinear coordinates) for net barotropic volume flux of $Q = 9600 \text{ m}^3/\text{s}$

features are rather well known from observations (Latif et al. 1991, Gregg and Özsoy 2002) and also meticulously have been documented more than three centuries ago by Marsili (1681).

Finally, water of Black Sea origin, with slightly increased salinity by mixing in the Strait, exits the Bosphorus in the form of a jet shooting directly south into the Marmara Sea. This initial straight southward orientation of the Bosphorus jet, noted in the earlier literature (Latif et al. 1991; Özsoy et al. 2001), is the result of the redirection towards the south by the channel mouth geometry, including the protruding headlands of Üsküdar and Sarayburnu (Scutari and Seraglio Point of the old Ottoman and Byzantium city). Asymmetrical horizontal shear evident in the velocity profile of the jet issuing into the Marmara Sea, with sharper gradients on the eastern side, implies negative vorticity export, which then sets the initial condition for the ensuing Marmara Sea circulation (Fig. 15c).

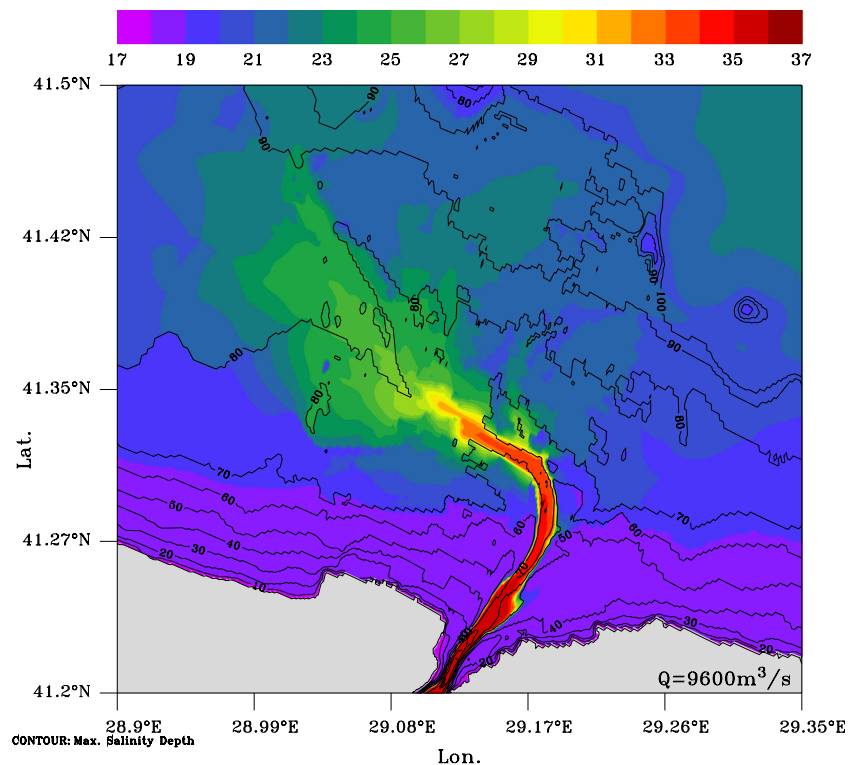
However, the negative vorticity export by the jet, anticipated from basic principles as referred to in

Section 3.1.2 can only be quantified by further 3D analyses of vorticity advection near the Bosphorus exit, in support of the generation of anticyclonic central gyre of the Marmara Sea. Since this is outside the present scope, we only note here that the successful representation of such essential features anticipated from theory and observations result from the full accounting of the strait physics in the present TSS model, which often are ignored by models that exclude the straits.

In the exit region of the Bosphorus on the Black Sea shelf (Fig. 16), the outflow details are sufficiently well captured, thanks to the adequate representation of the canyon topography and the sill within it, allowed by the horizontal resolution of the model. The outflow of the ‘Mediterranean effluent’ overflows the sill at a depth of $\sim 60 \text{ m}$ and is guided by the canyon and gets rapidly mixed with the overlying waters as it finally spreads on the shelf when the canyon becomes flatter, as also has been experienced in the related literature (Latif et al. 1991; Özsoy et al. 2001; Dorrell et al. 2016).

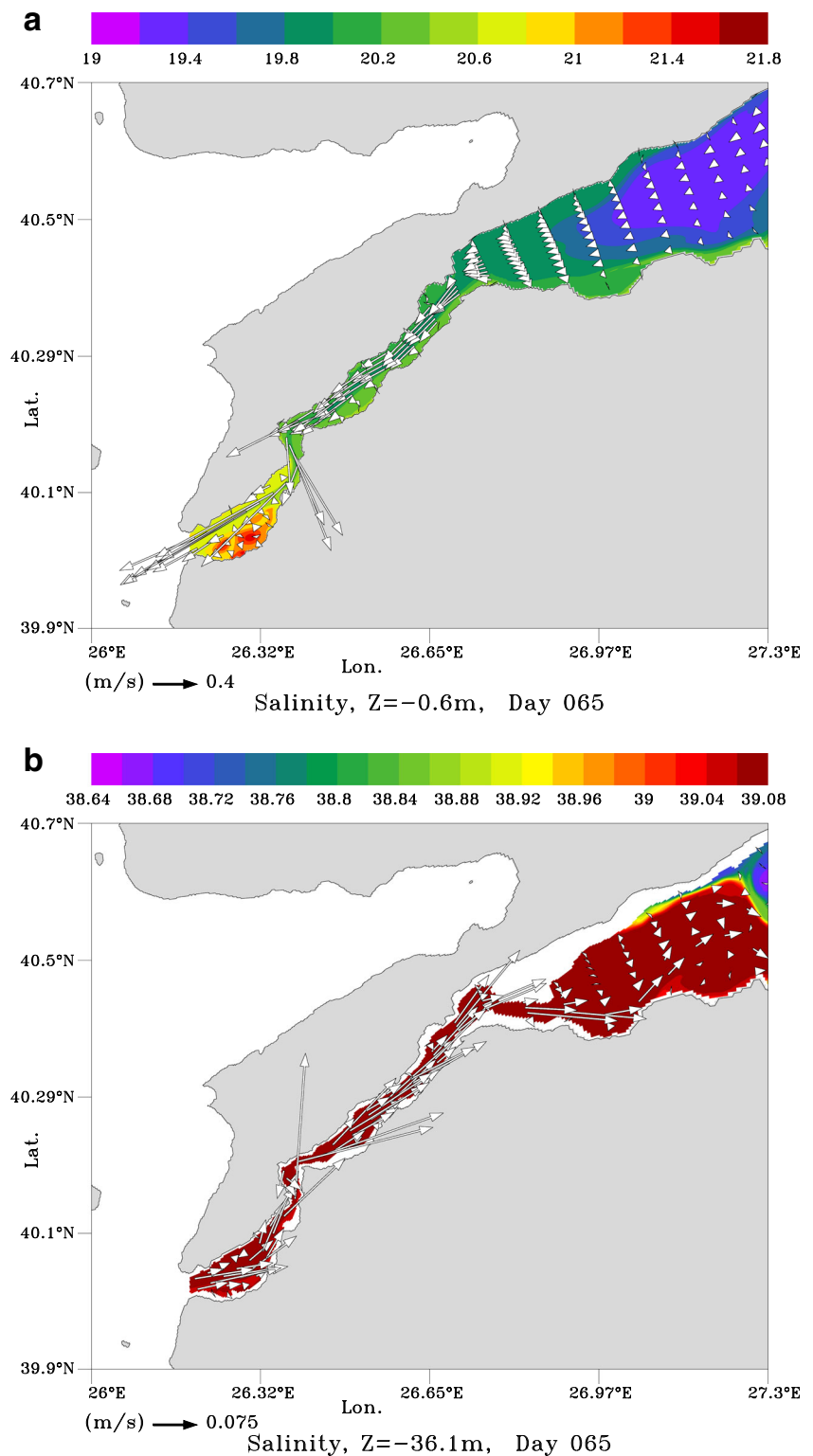
Similarly the salinity distribution and current vectors at depths of 0 m (surface) and 36 m in the Dardanelles are shown in Fig. 17a, b. The surface currents reorganize into a uniform stream entering the funnel section east of the Dardanelles Strait and meet the right angle turns of the channel at Nara Pass, where the width of the channel is also the narrowest (Fig. 17a), inducing the only hydraulic transition of the Strait, evident from the rapid change of the interface depth

Fig. 16 Maximum (bottom) salinity (colour) and depth (contours) adjacent to the Bosphorus Strait on the Black Sea continental shelf, for the net flux of $9600 \text{ m}^3/\text{s}$



Maximum Salinity, Day 065

Fig. 17 Salinity and current vectors at depths of **a** 0 m (surface) and **b** 36 m in the Dardanelles for net barotropic volume flux of $Q = 9600 \text{ m}^3/\text{s}$



(Fig. 9a–c) at this section. The surface salinity increases along the strait by mixing and entrainment into the surface layer from below, and makes a jump after Nara Pass in consequence to a dissipative region (hydraulic jump) past the narrows,

where the currents also increase because of the shallowing of the upper layer.

The lower layer flow entering from the Aegean Sea undergoes an opposite trend, speeding up after the narrows as

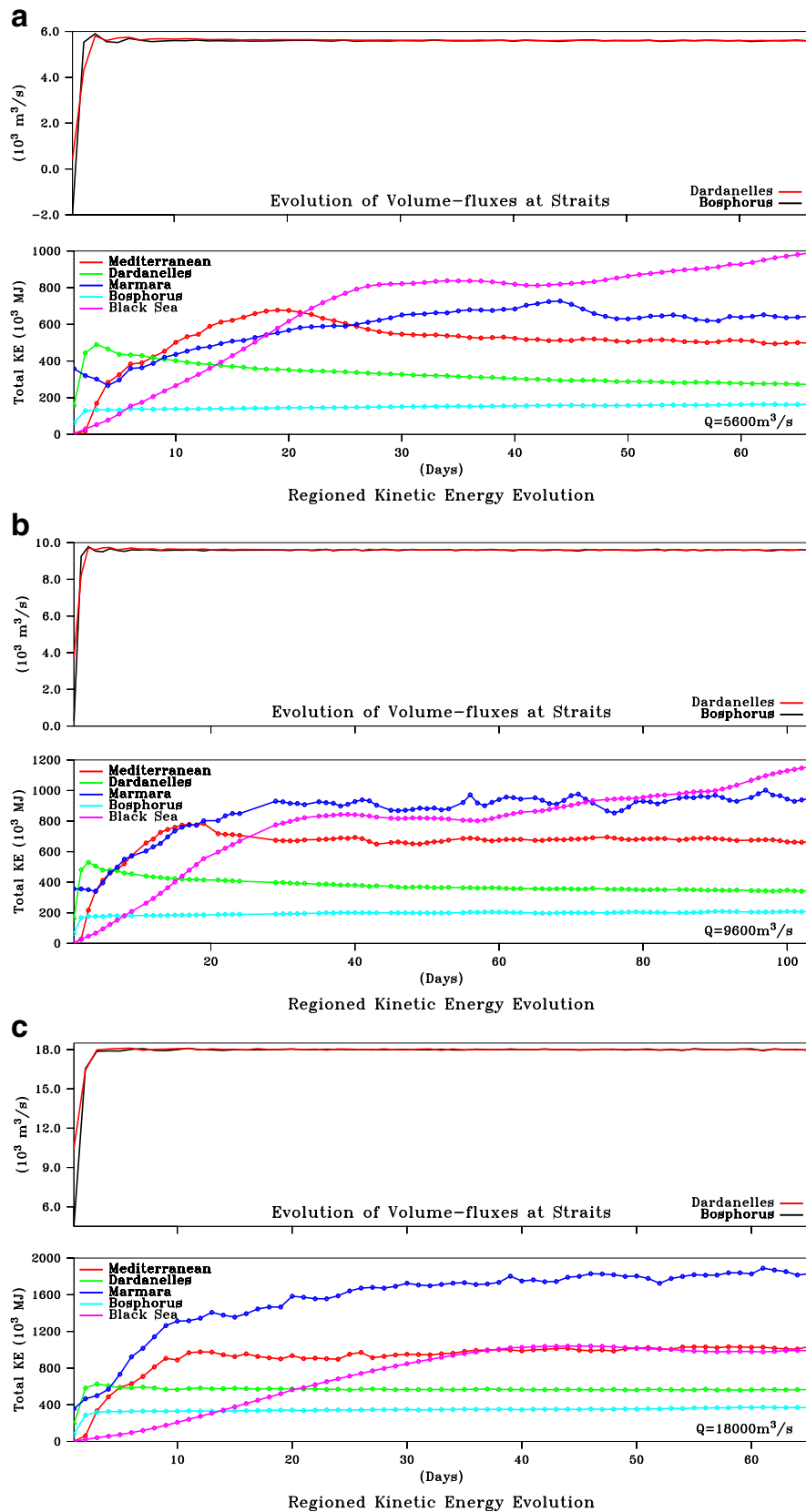


Fig. 18 Evolution of net flux in the Dardanelles and Bosphorus Straits and kinetic energy for different regions of the TSS for selected values of net transport, **a** $Q=5600$, **b** 9600 and **c** $18000 \text{ m}^3/\text{s}$

the lower layer thickness decreases (Fig. 17b), and the flow enters a deep cut canyon on the southern side of the funnel shaped eastern part of the Strait leading to the Marmara Sea.

3.2 Adjustment time scales

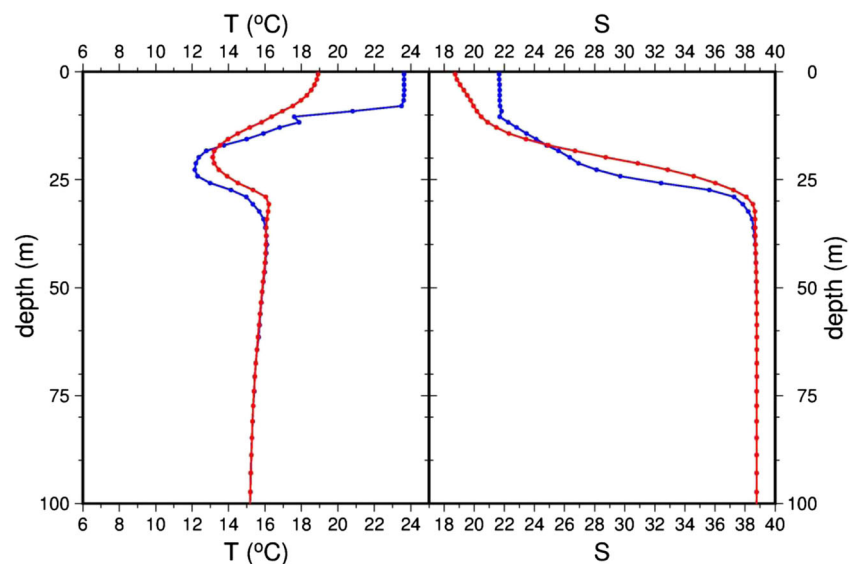
One particular finding of much interest, anticipated in view of the different scales of motion in the coupled system, is of great practical significance. Because the TSS has distinct regions of variations in geometrical properties and dynamical processes active in each of these regions, the physical response in terms of the kinetic energy levels is different in each region. Time-dependent evolution of the net flux and the kinetic energy are shown in Fig. 18a–c for different regions respectively for the three different sets of experiments corresponding to net fluxes of $Q = 5600, 9600$ and $18,000 \text{ m}^3/\text{s}$. It is observed that the net flux is established within days and thereafter controlled strictly by the net flux boundary condition. The approach to a steady state of the kinetic energy is always much faster in the two Straits, also being established in a few days after start-up, while the responses of the wider areas of the three adjacent basins are much slower. The adjustment to steady conditions is almost immediate, in about a single day, in the two Straits, while the Marmara Sea as a whole adjusts to a steady state in about a month.

The response of the Black Sea part of the model domain, which is much limited in size, is relatively slower and later departs from a steady state in most cases (Fig. 18a, b) except the last case, where the steady state is reached with the Bosphorus lower layer totally blocked (Fig. 18c). Because of the confined nature of the Black Sea domain, this

development is not of much concern in evaluating the TSS response in the mid-term, as the TSS seems to reach quasi-steady state conditions in about 2 months, and especially because the Straits, which isolate the TSS from the outward domains, reach steady state much earlier and remain constant afterwards.

We also evaluate in Fig. 19 how much the model ensures the property fields to reach steady state, by comparing temperature and salinity vertical profiles before and after the model run at the mid-Marmara station ($40^\circ 51' \text{N}$ $28^\circ 03' \text{E}$), shown in Fig. 4, which has been used to initialize properties in the basin. Initially a mixed layer is present in the data, showing uniform properties up to 10 m, which testifies to small wind-mixing effects. Remembering that no atmospheric effects are imposed in the model runs, one should not expect to find much agreement between the model and the initial results after the model adjustment process. Despite of this fact, quite good agreement is found between the model results and the initial observations after adjustment from a lock-exchange initial condition under the effect of a net flux of $9600 \text{ m}^3/\text{s}$, typical of the summer months (e.g. Özsoy et al. 2001). Although the exact flux value is not known at the time of the measurements, the basic structure of the profiles is conserved, save for the disappearance of the mixed layer; the cold intermediate layer and the sharpness of the halocline are preserved, indicating no excessive mixing has occurred. Despite the simplifying conditions omitting wind forcing, the model is faithful to the allowed physics within its proclaimed purpose to study the effects of the barotropic flux and stratified basin boundary conditions as sole factors driving the system.

Fig. 19 Temperature and salinity vertical profiles at station at ($40^\circ 51' \text{N}$ $28^\circ 03' \text{E}$) in the middle of Marmara Sea at initial time ($t = 0$, blue lines) and after the total length of the model run ($t = 103$ days, red lines), for a net flux of $9600 \text{ m}^3/\text{s}$



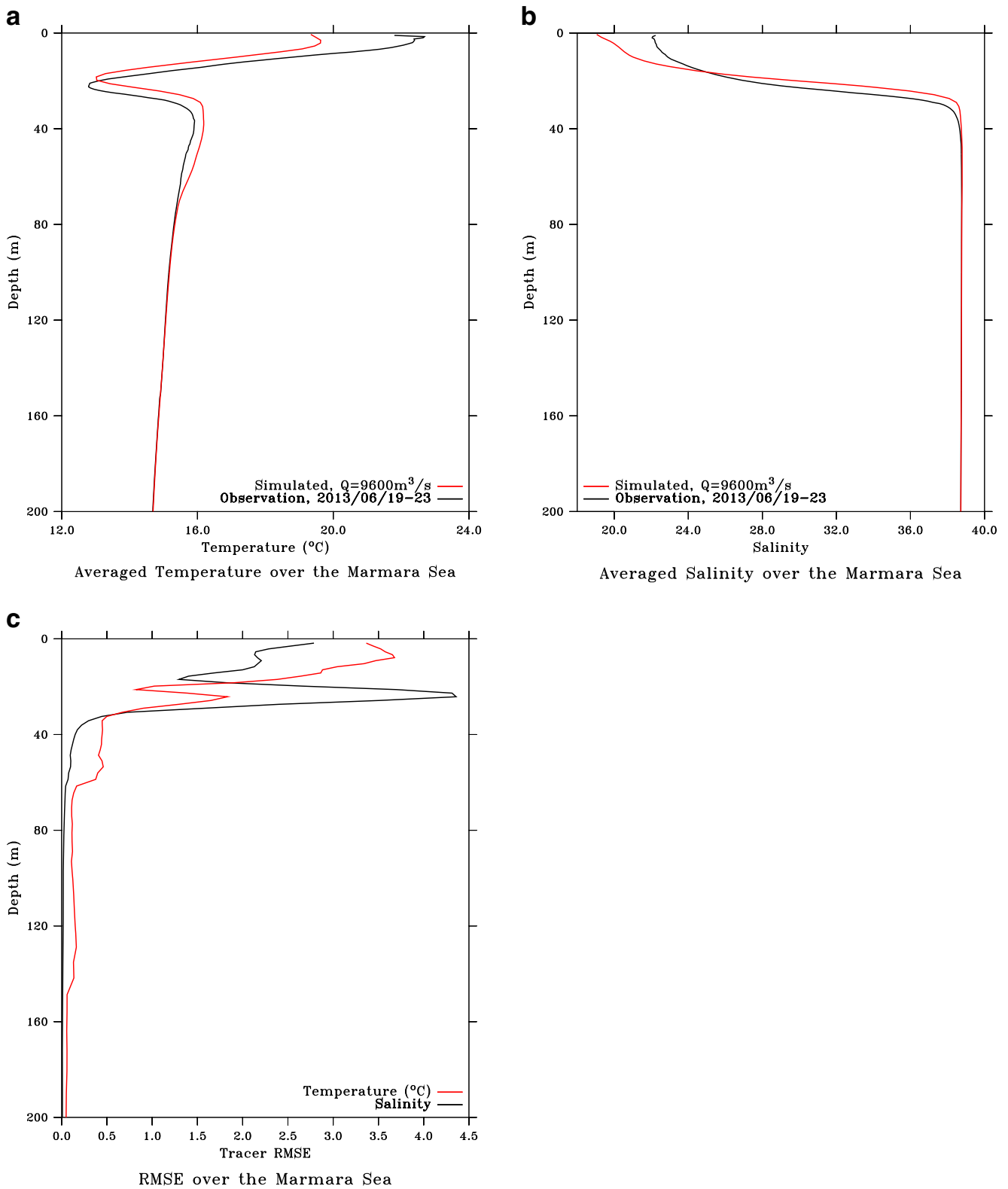


Fig. 20 Averaged **a** temperature and **b** salinity profiles obtained from the observations (black lines) and the model results (red lines), **c** rmse differences in temperature (red) and salinity (black) at Marmara Sea

CTD stations (only those inside the Marmara Sea proper in Fig.4) for a net flux of $Q = 9600\text{ m}^3/\text{s}$

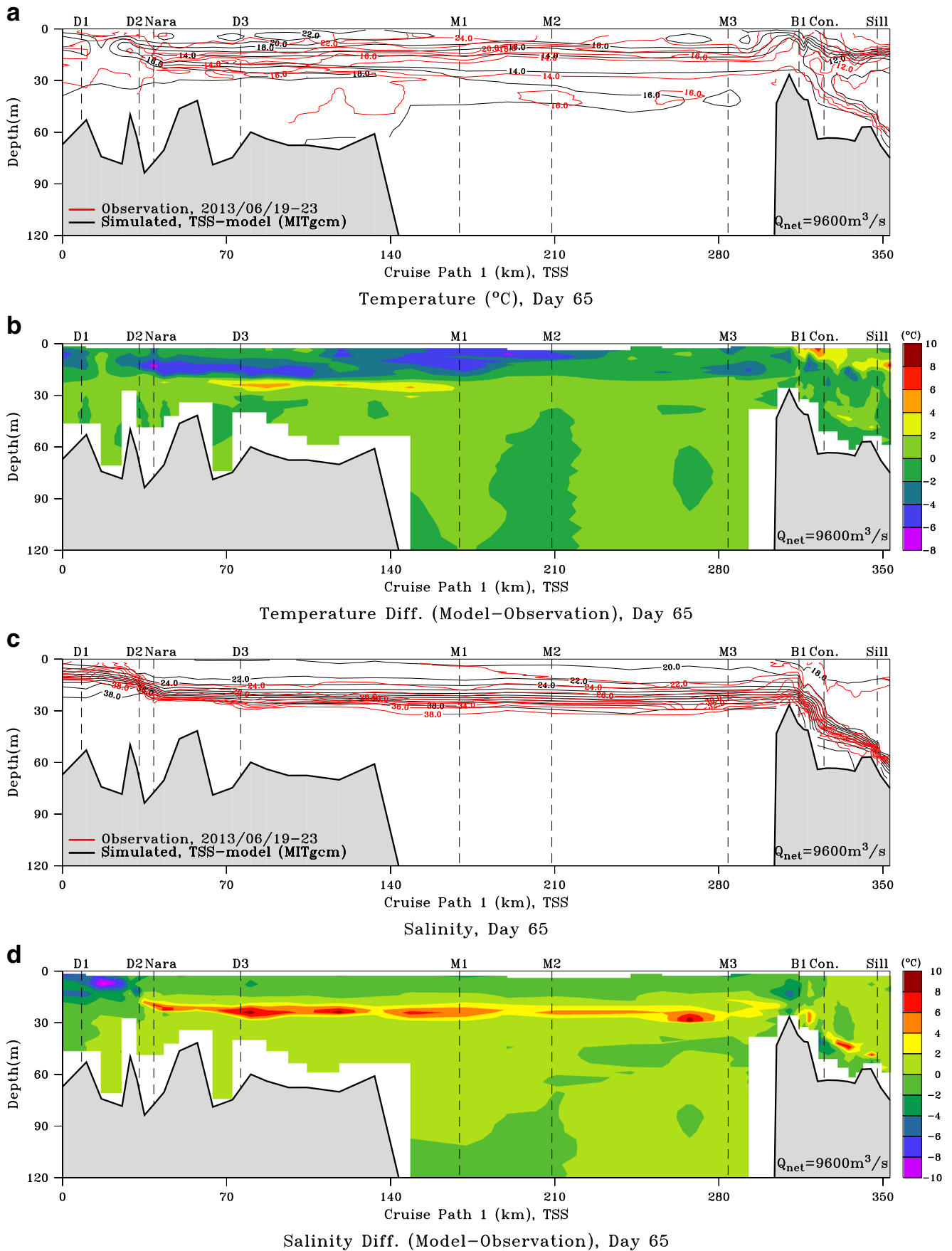


Fig. 21 Comparison of temperature (**a**, **b**) and salinity (**c**, **d**) along the TSS transect (*blue and green lines* in Fig. 4). Comparisons are made in **a** and **c** between fields of interpolated CTD data (*red contours*) and those obtained from the TSS model (*black contours*) for a net flux of $Q = 9600 \text{ m}^3/\text{s}$. The difference fields between CTD and model data are shown in (**b**) and (**d**)

3.3 Comparison with observations

We next compare model adjusted basin-wide conditions against observations in Fig. 20. For this purpose we have constructed average profiles of model and observed temperature and salinity (Fig. 20a, b) at the locations of CTD stations in Marmara Sea, a subset of those shown in Fig. 4, before and after the full length of the model run for the net flux of $9600 \text{ m}^3/\text{s}$. The TSS average (including the Marmara Sea) of root mean square difference (rmse) between observations and model results at CTD stations presented in Fig. 20c shows appreciable differences near surface. This is an expected result as surface flux boundary conditions have not been applied. The secondary increase in rmse at about 20–30 m depth occurs due to slightly misplaced interface in the model predictions, also expected in the absence of full correspondence of environmental conditions between model and observations.

Further comparisons are made in Fig. 21 between the temperature and salinity distributions of the observations in June 2013 with the TSS model results, plotted along the entire TSS transect following the line of mid-basin stations in Fig. 4.

It is shown in Fig. 21 that the main features of the observed fields are reasonably well recovered in the model simulated property fields. The differences between the observed and model fields are mainly in the vertical position and thickness of the interfacial layer. These differences are reasonable to expect, considering the synoptic environment including wind mixing, surface heat/salt fluxes not represented in the model but in reality expected to affect the finer-scale tracer advection-diffusion patterns. Focusing attention on the larger scale dynamical features, it is clearly visible that the model closely follows the observed fast variations inside the straits and their exit regions, as well as along the whole length of the Marmara Sea. In particular, from the positions and density of equally spaced contours for both the observational and model produced fields in Fig. 21a, c, it can be verified that the slight displacements in vertical position (appropriate for the sharp stratification) and representation of the thickness of the interface (a measure of interfacial mixing) are responsible for the differences between the two fields displayed in Fig. 21b, d. In fact, this is again the simplest validation of the faithful reproduction of dynamical and mixing processes by the model excluding the effects of surface fluxes. In fact, larger differences are found in the upper layer temperature (Fig. 21a, b) due to the omission of model surface fluxes, which are much smaller in the conservative salinity field (Fig. 21c, d), save for

errors resulting from the slight misplacement of the interface. Overall, these differences are consistent with those described earlier in Figs. 19 and 20.

Comparing results in Bosphorus, we find quite faithful reproduction of main features by the model, with appreciable temperature differences in the surface mixed layer, and salinity differences near the interface towards the north part where sharper interfacial gradients are noticeable in measurements, compared to the slightly greater interfacial mixing displayed in the model results. At the Dardanelles, the wide eastern part of the strait reflects the same conditions as Marmara Sea discussed above, while the western part, past the Nara Passage, shows some sensitivity, with a change in sign of the salinity anomaly, indicating that the upper layer becomes thinner in the west, with a deeper position of the model interface as compared to the observations; possibly implying faster exchange currents in the real world.

3.4 Comparison between TSS and Bosphorus models

The TSS model (MITgcm) results are compared with results from the Bosphorus model (ROMS) obtained by Sözer (2013) and presented in Sözer and Özsoy (2017). Only partial comparison is made based on models with essentially different parameterizations, boundary and initial conditions described elsewhere. In fact, a quantitative comparison would also not be appropriate, because of the different model domains covered by the Bosphorus model (with small end reservoirs for its boundaries) being only a subset of the TSS domain. The only reason we attempt such comparison is to test and verify our initial hypothesis that better results would be obtained by treating the TSS as an integral system of coupled elements including the straits, the Marmara Basin and the adjacent seas, rather than trying to build an understanding of system behaviour based on individual parts such as the Bosphorus represented as isolated elements in the coupled system.

There are also a number of common features of the two model systems that seem to support the essential hypothesis proposed. First of all, both models study the response to steady net barotropic flux without imposing transient atmospheric forcing. Briefly, the fine resolution Bosphorus model uses a topography following s-coordinate system in the vertical, with a minimum grid spacing of 50 m in the critical strait areas, 35 levels in the vertical, with specific mixing and turbulence schemes (Sözer 2013; Sözer and Özsoy 2017). The ROMS model has been largely successful in representing anticipated features such as hydraulic controls and mixing in the Bosphorus.

Although good comparison is obtained for varied net barotropic flux imposed on both models, only a particular comparison of Bosphorus salinity and temperature fields for $Q = 9600 \text{ m}^3/\text{s}$ is provided in Fig. 22. Despite the much greater resolution of the Bosphorus model and the much larger areal coverage of the TSS model, this model-model comparison is

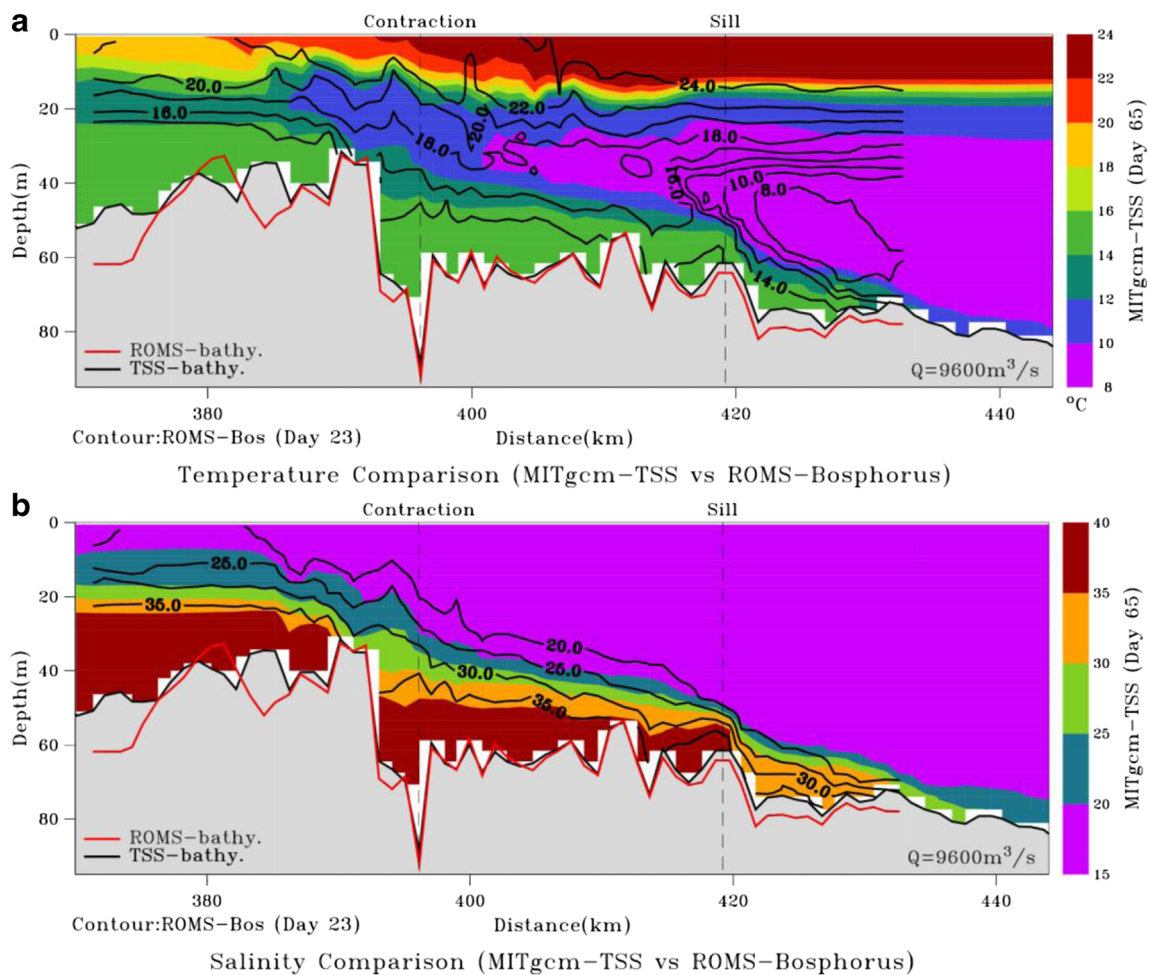


Fig. 22 Comparison of **a** temperature and **b** salinity along the Bosphorus produced by the TSS (MITgcm, colours) and Bosphorus (ROMS, contours) models for the net barotropic flux value of $Q = 9600 \text{ m}^3/\text{s}$

excellent, showing that most of the essential features, such as the hydraulic controls at the topographical barriers including the exit, contraction and sill of the Bosphorus (indicated by the criticality analysis presented earlier), the interface thickness, and the mixing properties are equally well represented in the TSS model, producing results comparable with the higher resolution, stand-alone Bosphorus model.

3.5 Overall comparison between TSS/Bosphorus models and observations

A synthesis of various end results is attempted in Fig. 23, comparing the Bosphorus upper layer (Q_1) and lower layer (Q_2) volume fluxes obtained from the TSS (MITgcm) model with those obtained from the Bosphorus model (ROMS) of Sözer (2013) and with observational data. The ADCP measurements referred to in Fig. 23 were collected during 1991–1995 on board R/V BİLİM of the IMS-METU by integrating continuous recordings of current velocity across sections of the Bosphorus (Özsoy et al. 1998). The Merz and Möller data were obtained by digitizing them from Fig. 2a of Maderich

et al. (2015) as the originals (Merz and Möller 1928; Möller 1928) could not be accessed.

Comparison between the two models indicates differences in the predicted layer fluxes in response to the imposed net flux. In general, the TSS model produces smaller fluxes in the individual layers as compared to the Bosphorus model of Sözer and Özsoy (2017), and are in better agreement with the measured values as indicated in Fig. 23. In principle, the differences could be arising from the different models and geographical domains used, as well as a series of other model parameters and schemes.

Estimates of net flux required for the blocking of the layer flows can be obtained from Fig. 23, roughly corresponding to $30,000 \text{ m}^3/\text{s}$ for the lower layer and $-20,000 \text{ m}^3/\text{s}$ for the upper layer, confirmed by the available data and consistent with the estimates of two well-resolved numerical models. The estimate for the lower layer blocking is in agreement with the simplified 1D two-layer numerical model of Oğuz et al. (1990), estimating the value at $26,000 \text{ m}^3/\text{s}$. In comparison, a simpler calculation in the same paper, based on the Farmer and Armi (1986) formulation for frictionless flow produced

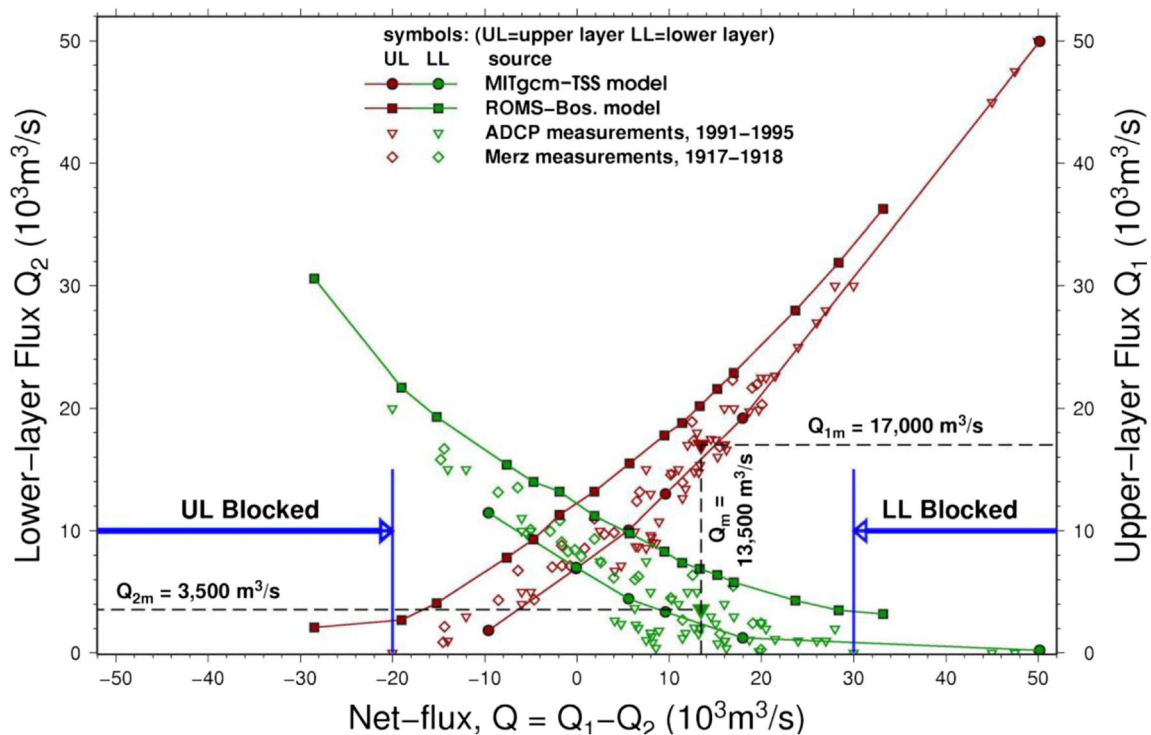


Fig. 23 Upper layer (Q_1) and lower layer (Q_2) volume fluxes through the Bosphorus as a function of the net flux ($Q = Q_1 - Q_2$), based on past observational data and compared with the results from two different model systems: the Bosphorus model (ROMS) of Sözer (2013) and Sözer and Özsoy (2017) and the present TSS (MITgcm) model. The

average upper, lower layer and net flux values Q_{1m} , Q_{2m} and Q_m , respectively shown by dashed lines are the average values obtained from the ADCP measurements (Özsoy et al. 1998). The blue arrows indicate limiting values of net flux corresponding to upper or lower layer blocking, based on observational and modelling evidence

much larger values of 25,000–46,000 m^3/s for lower layer blocking and a blocking flux value of $-65,000 \text{ m}^3/\text{s}$ for the upper layer, far outside the reasonable range displayed in Fig. 23 predicted by the turbulence and bottom friction parameterization used in the 3D Bosphorus and TSS models.

Between the two models constructed using the ROMS and the MITgcm, the Bosphorus model seems to have larger mixing, evident in the thicker interface, demonstrated in the last section. Yet, although the Bosphorus model is more specific to the Strait and has better resolution, the TSS model seems to perform even better in comparison with

observations, with a greater number of past observations clustered around the TSS model solution.

The comparison of fluxes corresponding to net flux values tested in the TSS model is reviewed in Table 1. The model flux values displayed have been obtained at the middle of the Strait, and observations are also from sections close to the middle of the Strait. The layer fluxes compared between the two straits, the Dardanelles and Bosphorus, in the case of the TSS model indicates large differences, with the upper layer flux being much larger in the Dardanelles as compared to the Bosphorus for lower values of net flux; the lower layer flux becoming much larger for

Table 1 Upper, lower layer and total fluxes at straits based on integrated tss and stand-alone bosphorus models

Net flux Q (m^3/s)	Bosphorus (TSS) (m^3/s)		Dardanelles (TSS) (m^3/s)		Bosphorus (ROMS) (m^3/s)	
	Upper Q_1	Lower Q_2	Upper Q_1	Lower Q_2	Upper Q_1	Lower Q_2
-9600	1900	11,500	3500	13,100	6800	16,400
0	6950	6950	8750	8750	12,200	12,200
5600	9950	4550	13,200	7600	15,400	9800
9600	13,000	3400	15,800	6200	17,800	8200
18,000	19,200	1200	22,100	4100	23,600	5600
50,000	50,100	100	52,700	2700	—	—

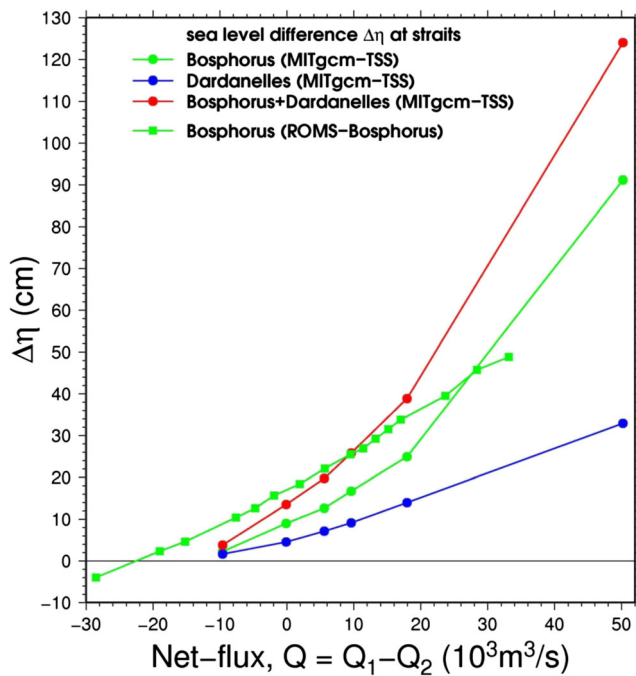


Fig. 24 Comparison of sea level difference between the ends of the Bosphorus and Dardanelles Straits obtained from the TSS (MITgcm) and the stand-alone Bosphorus (ROMS, Sözer and Özsoy 2017) models with respect to the net flux Q

the higher net flux values. Therefore, both the amounts and the ratios of fluxes between the two straits and between the layers change with the net flux. The layer fluxes being greater at Dardanelles compared to Bosphorus in the TSS model is a consequence of the mixing and entrainment achieved in the two straits and in transit through the Marmara Sea.

In comparison to the TSS model results, the stand-alone Bosphorus model with the same net fluxes produces larger layer fluxes. The fact that larger fluxes are produced despite the evidence for greater mixing in the Bosphorus model indicated in the last section implies that the difference is mainly because of the greater domain used in the TSS model investigating the coupled behaviour rather than the individual elements. The better agreement of the TSS model with the observations in Fig. 23 suggests that the need for coupled modelling is clearly

recognized—in fact, it shows that the motivation for integrated modelling of the TSS is essential for better representation of the system dynamics.

We also attempt an initial synthesis of sea level difference created across the straits based on the existing model results in Fig. 24. The individual sea level differences across the Bosphorus and Dardanelles Straits produced by the TSS model and those calculated for the Bosphorus based on the stand-alone Bosphorus model are presented. While a linear increase in sea level difference is obtained from the Bosphorus model, a non-linear response is produced in the TSS model; in this case the Bosphorus sea level difference inordinately rising to large values under extreme net flux values leading to blocked flows. The linear increase in sea level predicted by the stand-alone Bosphorus model of Sözer and Özsoy (2017) is similar to the results of Oğuz et al. (1990) and in fact quantitatively almost the same, while the nonlinear behaviour is qualitatively and quantitatively very different for the TSS model. This difference in behaviour is implicative of advantages of the integral response of the TSS, including the interactive contributions of the system elements, the two Straits and the Marmara Sea interior with its modified circulation summarized in Fig. 6 playing their parts in contribution to the end result, with radical changes in them occurring especially after the onset of blocking conditions in the Bosphorus under increased net fluxes.

The sea level differences that develop at the two straits, Bosphorus and Dardanelles are given in Table 2 in relation to net barotropic flux and the values obtained from the TSS model are compared with the model results for the Bosphorus (Sözer 2013). While the total range of sea level in the Marmara Sea between cyclonic and anticyclonic areas varies between 2 and 12 cm (Fig. 6), the net sea level differences across the straits are much larger, varying between 2 and 91 cm in the Bosphorus and 2–33 cm in the Dardanelles. These results imply sea level differences in the range of about 0–120 cm between the Black Sea and the Aegean Sea, for the imposed range of net transport.

Table 2 Sea level difference versus net flux at straits based on integrated tss and stand-alone bosphorus models

Net flux Q (m^3/s)	Bosphorus (TSS) sea level difference $\Delta\eta$ (cm)	Dardanelles (TSS) sea level difference $\Delta\eta$ (cm)	Bosphorus (ROMS) sea level difference $\Delta\eta$ (cm)
−9600	2.2	1.6	8.9
0	9.0	4.5	16.9
5600	12.6	7.1	22.0
9600	16.7	9.1	25.6
18,000	24.9	13.9	34.6
50,000	91.1	32.9	—

The comparison between models for the case of the Bosphorus indicates larger sea level difference in the stand-alone model compared to the TSS model. This again is most likely a result of the better represented coupling effects introduced by the TSS model. Yet, this needs to be verified further with continuing investigations.

4 Discussion and conclusions

This work represents the first attempts in understanding, by means of numerical simulation, the water circulation in the TSS as a whole, emphasizing the coupling between the Marmara Sea and the adjoining seas through elongated, narrow straits.

In addition to the general circulation features, fine-scale dynamics predicted by the TSS model are interpreted and compared with observations for the first time. The ultimate aim of resolving the umbilical Bosphorus and Dardanelles Straits connecting the Aegean, Marmara and Black Sea basins have been achieved and appears to provide the added value expected of the integral behaviour of the coupled system, while also capably and accurately predicting the fine-scale physical behaviour of the straits themselves.

One of the important results of this research, also supported by earlier observations, is the selective controls of its multi-scale coupled dynamics. In particular, due to its unique maximal exchange regime, the Bosphorus Strait leads the common response of the TSS. As the most restrictive element in the TSS, the Bosphorus plays a dominant role in the system thanks to the critical transitions at hydraulic controls, analysed by Sözer and Özsoy (2017) and in the present work. Both the Bosphorus and Dardanelles Straits have a much faster response compared to the rest of the TSS, clearly setting up the response in the beginning of the simulation, while the rest of the system slowly adjusts to conditions imposed on them by the two straits.

It is clearly observed in the model results that the Bosphorus Jet discharging into the confined space of the Marmara Sea determines the subsequent evolution of its surface circulation and has a special role in the mixing processes. For medium values of the net water flux through the system, the jet shoots south from the Strait, later to bend westward and join the central anticyclone that is created in the middle of the Marmara Sea possibly by the export of negative vorticity from the Bosphorus, although this is not yet quantified and should be the subject of further study. The flow after the anticyclone follows the northern coast towards the Dardanelles Strait. Significant changes occur for increasing values of the net flux when the Bosphorus lower layer flow becomes blocked. The Bosphorus Jet originally circulating around the anticyclone is receded east to become attached to the western coast of the Bosphorus, while a cyclonic gyre replaces the former location of the central anticyclone while an anticyclonic circulation is

created to its west. The changes in the circulation appear linked to changes in vertical structure of density and interface depth which is observed to switch to deeper level in blocked flow conditions, thereby changing the vorticity input from the strait. This nonlinear behaviour regarding changes in circulation demonstrates one of the unique advantages of the integrated modelling of the TSS.

The lower layer inflow through the Dardanelles enters the Marmara Sea trapped below the pycnocline. These features are only indicative of the initial development, since steady state conditions for the lower layer are not reached in the model, and are not expected to occur before many years. Earlier studies not described in the present context refer to variable characteristics (Beşiktepe et al., 1993, 1994, Hüsrevoğlu, 1999) depending on Aegean Sea water density, resulting in the Dardanelles inflow to either transit below the pycnocline or sink to the bottom of the western basin of the Marmara Sea.

Because the model results apply to steady state conditions, the mean annual or seasonal circulation features under atmospheric forcing could be diversely different from those described here under net volume flux forcing. The general description of the predicted S-shaped current system of the Marmara Sea appears valid during calm summer conditions (e.g. Beşiktepe et al. 1993, 1994; Demyshev and Dovgaya 2007), while it seems to break up to smaller scale elements during winter or whenever other external forcing becomes active.

In terms of exchange fluxes and sea level difference across the TSS, integral modelling of the TSS seems to have clear advantages over separate models of the basin and strait elements. This is especially clear when comparing sea level differences obtained from integrated and stand-alone models with respect to net barotropic flow. The sea level difference across the stand-alone model of the Bosphorus is found to be larger than that produced by the integrated TSS model, comparable in magnitude with the total sea level difference across the entire TSS including both Straits. The difference appears to be mainly due to the different modelling approaches, disregarding few inescapable differences of grid structure and parameterizations in the individual models.

There are also qualitative differences between the sea level response of the different models compared. The sea level difference obtained from the stand-alone model has a linear variation with net flux, shown to be comparable to other isolated strait models, while the integrated TSS model with straits coupled to the Marmara Sea and adjacent basins produces a much different nonlinear response which actually deviates even more strongly from a linear behaviour when the flow in the Bosphorus becomes blocked. The same is observed for the circulation in the Marmara Sea, which varies nonlinearly with the net flux to switch from an anticyclonic central gyre to confined series of smaller gyres when the flow becomes blocked. These results point to the positive

advantages of the integrated modelling which defines the completely different dynamical behaviour of the coupled system compared to stand-alone models.

Further model simulations are necessary to describe the mid- and long-term processes governing transport and mixing in the TSS. For instance, the steady simulations reviewed here for either the TSS or the individual Bosphorus Strait do not say anything about the transient response that could be very different and infinitely more complex. Furthermore, these early results also indicate that the models used for the TSS, being actually a small piece of the ocean, should have all the advanced physics that are now being introduced into a new generation of ocean models: nonlinear free surface, non-hydrostatic, turbulence parameterizations, selective horizontal and vertical mixing and diffusion processes, surface and bottom boundary layers, improved air-sea interaction, which are all very important in coastal environments, an extreme example of which is the TSS.

Aspects of these new findings and other immediate research questions could be further investigated taking advantage of the new generations of computational models and infrastructure.

Acknowledgements This study was made possible under the bilateral research project 111Y308 entitled ‘Dynamics of high Energy Environment: Processes at the Turkish Straits System (DEEP)’ supported by the Turkish Scientific and Technical Research Council (TÜBİTAK) and the Italian Foreign Ministry during 2012–2015.

The dedicated computing resources for carrying out the model runs have been provided by the PRACE Distributed European Computing Initiative (DECI-10) under the PRACE-2IP project (FP7 RI-283493) during 2013/2014. The computations have been performed on the IBM Power 775 (called Boreasz) installed at the Maciej Cytowski, ICM, University of Warsaw, Poland. The theoretical performance of Boreasz are about 8 flops/core \times 3.83 Ghz \times 32 cores/node \times 80 nodes = 78.43 Teraflops. The time necessary to perform 1 day of simulations was approximately 1 h of computer time when 768 cores were used. The very good performance of the Boreasz supercomputer at the University of Warsaw, Poland in addition to the other computing resources used at the host Institutions of the researchers at ENEA (CRESCO/ENEAGRID High Performance Computing infrastructure and its staff), Italy and IMS-METU, Turkey have contributed to the success of this study. We also extend our thanks to the captains and technicians of the R/V BİLİM and the research personnel of the IMS-METU for their efforts.

References

- Altıok H, Kayışoğlu M (2015) Seasonal and interannual variability of water exchange in the strait of Istanbul. *Medit Mar Sci* 16(3):636–647
- Androulidakis YS, Kourafalou VH, Krestenitis YN, Zervakis V (2012a) Variability of deep water mass characteristics in the North Aegean Sea: the role of lateral inputs and atmospheric conditions. *Deep-Sea Res Part I Oceanogr Res Pap* 67:55–72
- Androulidakis YS, Krestenitis YN, Kourafalou VH (2012b) Connectivity of the North Aegean circulation to the Black Sea water budget. *Cont Shelf Res* 48:8–26
- Beardsley RC, Hart J (1978) A simple theoretical model for the flow of an estuary on to a continental shelf. *J Geophys Res* 83:873–883
- Beşiktepe Ş, Özsoy E, Ünlüata Ü (1993) Filling of the Marmara Sea by the Dardanelles lower layer inflow. *Deep-Sea Res* 40:1815–1838
- Beşiktepe Ş, Özsoy E, Latif MA, Oğuz T (2000). Marmara Denizi'nin Hidrografisi ve Dolaşımı (Hydrography and Circulation of the Marmara Sea). In: Öztürk B et al. (eds) Marmara Sea 2000 Symposium Book. TÜDAV Publication, İstanbul, (in Turkish)
- Beşiktepe Ş, Sur Hİ, Özsoy E, Latif MA, Oğuz T, Ünlüata Ü (1994) The circulation and hydrography of the Marmara Sea. *Prog Oceanogr* 34:285–334
- Blain CA, Cambazoğlu MK and Kourafalou VH (2009) Modeling the Dardanelles strait outflow plume using a coupled model system, OCEANS 2009, MTS/IEEE Biloxi—Marine Technology for Our Future: Global and Local Challenges, pp.1–8
- Bleck R, Boudra D (1981) Initial testing of a numerical ocean circulation model using a hybrid (quasi-isopycnic) vertical coordinate. *J Phys Oceanogr* 11:755–770
- Book JW, Ewa Jarosz E, Chiggiato J, Beşiktepe Ş (2014) The oceanic response of the Turkish Straits System to an extreme drop in atmospheric pressure. *J Geophys Res* 119:3629–3644
- Carillo A, Sannino G, Artale V, Ruti PM, Calmanti S, Dell'Aquila A (2012) Steric Sea level rise over the Mediterranean Sea: present climate and scenario simulations. *Clim Dyn* 39(9–10):2167–2184
- Chiggiato J, Jarosz E, Book JW, Dykes J, Torrisi L, Poulain P-M, Gerin R, Horstmann J, Beşiktepe Ş (2011) Dynamics of the circulation in the sea of Marmara: numerical modeling experiments and observations from the Turkish straits system experiment. *Ocean Dyn* 62(1):139–159
- Defant A (1961) *Physical Oceanography*, Pergamon Press, London, 1961. Vol. 1, pp. xvi + 729; Vol. 2, pp. viii + 598
- Delfanti R, Özsoy E, Kaberi H, Schirone A, Salvi S, Conte F, Tsabarıs C, Papucci C (2013) Evolution and fluxes of ¹³⁷Cs in the Black Sea/Turkish Straits System/North Aegean Sea. *J. Mar. Sys.* 135:117–123
- Demirov E, Pinardi N (2002) Simulation of the Mediterranean Sea circulation from 1979 to 1993: Part I. The interannual variability. *J. Mar. Sys.* 33–34:23–50
- Demyshev SG, Dovgaya SV (2007) Numerical experiment aimed at modeling the hydrophysical fields in the Sea of Marmara with regard for Bosphorus and Dardanelles. *Phys Oceanogr* 17(3):141–153
- Demyshev SG, Dovgaya SV, Ivanov VA (2012) Numerical modeling of the influence of exchange through the Bosphorus and Dardanelles Straits on the hydrophysical fields of the Marmara Sea, *Izvestiya. Atmospheric and Oceanic Physics* 48(4):418–426
- Dorrell RM, Peakall J, Sumner EJ, Parsons DR, Darby SE, Wynn RB, Özsoy E, Tezcan D (2016) Flow dynamics and mixing processes in hydraulic jump arrays: implications for channel-lobe transition zones. *Mar Geol* 381:181–193
- Farmer DM, Armi L (1986) Maximal two-layer exchange over a sill and through the combination of a sill and contraction with barotropic flow. *J Fluid Mech* 164:53–76
- Göktaşan E, Tur H, Ecevitoglu B, Görüm T, Türker A, Tok B, Çağlak F, Birkan H, Şimşek M (2005) Evidence and implications of massive erosion along the Strait of İstanbul (Bosphorus). *Geo-Mar Lett* 25: 324–342
- Göktaşan E, Ergin M, Özyalvaç M, Sur Hİ, Tur H, Görüm T, Ustaömer T, Batuk FG, Alp H, Birkan H, Türker A, Gezgın E, Özturan M (2007) Factors controlling the morphological evolution of the Çanakkale Strait (Dardanelles, Turkey). *Geo-Mar Lett* 28:107–129
- Gregg MC, Özsoy E, Latif MA (1999) Quasi-steady exchange flow in the Bosphorus. *Geophys Res Lett* 26:83–86
- Gregg MC, Özsoy E (1999) Mixing on the Black Sea shelf north of the Bosphorus. *Geophys Res Lett* 26:1869–1872
- Gregg MC, Özsoy E (2002) Flow, water mass changes and hydraulics in the Bosphorus. *J Geophys Res* 107(C3). doi:10.1029/2000JC000485

- Gündüz M, Özsoy E (2015) Blocking of the upper layer flow in the Dardanelles Strait and its influence on fish catches. *J. Black Sea/Mediterranean Environment* 21(3):250–263
- Gündüz M (2016) Possible recovery site of four non-recovered bodies lost in the Marmara Sea by using an ocean circulation model. *Australian Journal of Forensic Sciences*. doi:10.1080/00450618.2016.1138320
- Gürses Ö, Aydoğdu A, Pinardi N, Özsoy E (2016). A Finite Element Modeling Study of the Turkish Straits System, in Özsoy E et al. (editors), *The Sea of Marmara—Marine Biodiversity, Fisheries, Conservation and Governance*, Turkish Marine Research Foundation (TÜDAV) Publication #42
- Hundsdoerfer W, Koren B, Vanloon M, Verwer J (1995) A positive finite-difference advection scheme. *J Comput Phys* 117(1):35–46
- Huq P (2013) Buoyant Outflows to the Coastal Ocean, in: H. J. S. Fernando (ed.), *Handbook of Environmental Fluid Dynamics*, Volume One, CRC Press/Taylor & Francis Group, LLC, 1,207–215
- Hüsrevoğlu YS (1999) Modelling of the Dardanelles Strait lower-layer flow into the Marmara Sea, M.Sc. Thesis, Institute of Marine Sciences, METU, Erdemli, Mersin, Turkey
- Ilıcak M, Özgökmen TM, Özsoy E, Fischer PF (2009) Non-hydrostatic modeling of exchange flows across complex geometries. *Ocean Modeling* 29:159–175
- Jarosz E, Teague WJ, Book JW, Beşiktepe Ş (2011a) On flow variability in the Bosphorus Strait. *J Geophys Res* 116:C08038. doi:10.1029/2010JC006861
- Jarosz E, Teague WJ, Book JW, Beşiktepe Ş (2011b) Observed volume fluxes in the Bosphorus Strait. *Geophys Res Lett* 38:L21608. doi:10.1029/2011GL049557
- Jarosz E, Teague WJ, Book JW, Beşiktepe ŞT (2012) Observations on the characteristics of the exchange flow in the Dardanelles Strait. *J Geophys Res* 117:C11012. doi:10.1029/2012JC008348
- Jarosz E, Teague WJ, Book JW, Beşiktepe ST (2013) Observed volume fluxes and mixing in the Dardanelles Strait. *J Geophys Res Oceans* 118:5007–5021. doi:10.1002/jgrc.20396
- Jordà G, Von Schuckmann K, Josey SA, Caniaux G, García-Lafuente J, Sammartino S, Özsoy E, Polcher J, Notarstefano G, Poulain P-M, Adloff F, Salat J, Naranjo C, Schroeder K, Chiggiato J, Sannino G, Macias D (2016) The Mediterranean Sea heat and mass budgets: estimates, uncertainties and perspectives (submitted for publication in *Progress in Oceanography*)
- Kanarska Y, Maderich V (2008) Modelling of seasonal exchange flows through the Dardanelles Strait. *Estuar Coast Shelf Sci* 79:449–458
- Kokkos N, Sylaios G (2016) Modeling the buoyancy-driven Black Sea Water outflow into the North Aegean Sea. *Oceanologia* 58:103–116
- Latif MA, Özsoy E, Oğuz T, Ünlüata Ü (1991) Observations of the Mediterranean inflow into the Black Sea. *Deep-Sea Res* 38(Suppl. 2): 711–723
- Lee B-S, Bullister JL, Murray JW, Sonnerup RE (2002) Anthropogenic chlorofluorocarbons in the Black Sea and the Sea of Marmara. *Deep Sea Res* 49:895–913
- Leith C (1968) Parameterization of vertical mixing in numerical models of tropical oceans. *Phys Fluids* 10:1409–1416
- Maderich VS (1998) Modelling of Mediterranean system-changes under climate variations and human impact. *Environ Model Softw* 13:405–412
- Maderich V, Ilyin Y, Lemesko E (2015) Seasonal and interannual variability of the water exchange in the Turkish Straits System estimated by modelling. *Medit Mar Sci* 16(2):444–459
- Marshall J, Hill C, Perelman L, Adcroft A (1997a) Hydrostatic, quasi-hydrostatic, and nonhydrostatic ocean modeling. *J Geophys Res Oceans* 102(C3):5733–5752
- Marshall J, Adcroft A, Hill C, Perelman L, Heisey C (1997b) A finite-volume, incompressible Navier Stokes model for studies of the ocean on parallel computers. *J Geophys Res Oceans* 102(C3): 5753–5766
- Marsili LF (1681) Osservazioni Intorno al Bosforo Tracio ovvero Canale di Constantinopoli, Rappresentate in Lettera alla Sacra Real Maestà Cristina Regina di Svezia da Luigi Ferdinando Marsigli. Nicolò Angelo Tinassi, Roma
- Mavropoulou A-M, Mantziafou A, Jarosz E, Sofianos S (2016) The influence of Black Sea Water inflow and its synoptic time-scale variability in the North Aegean Sea hydrodynamics. *Ocean Dyn* 66:195–206
- McKiver WJ, Sannino G, Braga F, Bellafiore D (2016) Investigation of model capability in capturing vertical hydrodynamic coastal processes: a case study in the north Adriatic Sea. *Ocean Sci* 12:51–69. doi:10.5194/os-12-51-2016
- Merz A, Möller L (1928). *Hydrographische Untersuchungen in Bosporus und Dardanelen*, Alfred Merz. Bearb. von Lotte Möller, Berlin : E. S. Mittler & Sohn, 1 Atlas of 16 charts, 3 figures, 8 tables of sizes 47 × 39 cm and text 133p
- Morrison A (2011) Upstream basin circulation of rotating, hydraulically controlled flows, 2011 Summer Program in Geophysical Fluid Dynamics, WHOI, 429 pp
- Möller L (1928) Alfred Merz' hydrographische untersuchungen in Bosporus und Dardanelen, *Veroff. Inst. Meerskunde Univ. Berlin. Neue Folge*, A., 18, 284 pp
- Naranjo C, Garcia-Lafuente J, Sannino G, Sanchez-Garrido JC (2014) How much do tides affect the circulation of the Mediterranean Sea? From local processes in the Strait of Gibraltar to basin-scale effects. *Prog Oceanogr* 127:108–116
- Nof D (1978a) On geostrophic adjustment in Sea Straits and wide estuaries: theory and laboratory experiments. Part I—one-layer system. *J. Phys. Ocean.* 8:690–702
- Nof D (1978b) On geostrophic adjustment in Sea Straits and wide estuaries: theory and laboratory experiments. Part II—two-layer system. *J. Phys. Ocean.* 8:861–872
- Oğuz T, Sur Hİ (1989) A two-layer model of water exchange through the Dardanelles Strait. *Oceanology Acta* 12:23–31
- Oğuz T, Özsoy E, Latif MA, Sur Hİ, Ünlüata Ü (1990) Modelling of hydraulically controlled exchange flow in the Bosphorus Strait. *J Phys Oceanogr* 20:945–965
- Oğuz T (2005) Hydraulic adjustment of the Bosphorus exchange flow. *Geophys Res Letters* 32:L06604. doi:10.1029/2005GL022353
- Özsoy E, Altok H (2016a). A Review of Hydrography of the Turkish Straits System, in Özsoy E et al. (editors), *The Sea of Marmara—Marine Biodiversity, Fisheries, Conservation and Governance*, Turkish Marine Research Foundation (TÜDAV) Publication #42
- Özsoy E, Altok H (2016b) A Review of Water Fluxes across the Turkish Straits System, in Özsoy E et al. (editors), *The Sea of Marmara—Marine Biodiversity, Fisheries, Conservation and Governance*, Turkish Marine Research Foundation (TÜDAV) Publication #42
- Özsoy E, Rank D, Salihoğlu İ (2002) Pycnocline and deep mixing in the Black Sea: stable isotope and transient tracer measurements. *Estuar Coast Shelf Sci* 54(3):621–629
- Özsoy E, Latif MA, Tuğrul S, Ünlüata Ü (1995) Exchanges with the Mediterranean, fluxes and boundary mixing processes in the Black Sea, In: F. Briand, (editor), *Mediterranean Tributary Seas*, Bulletin de l'Institut Océanographique, Monaco, Special Number 15, CIESM Science Series No. 1, Monaco p. 1–25
- Özsoy E, Latif MA, Sur Hİ, Goryachkin Y (1996) A review of the exchange flow regimes and mixing in the Bosphorus Strait, in: F. Briand, (editor), *Mediterranean Tributary Seas*, Bulletin de l'Institut Océanographique, Monaco, Special Number 17, CIESM Science Series No. 2, Monaco
- Özsoy E, Ünlüata Ü (1997) Oceanography of the Black Sea: a review of some recent results. *Earth Sci Rev* 42(4):231–272
- Özsoy E, Ünlüata Ü (1998) The Black Sea. In: Robinson AR, Brink K (eds) *The sea: the Global Coastal Ocean: Regional Studies and Syntheses*, 11. John Wiley and Sons, New York, pp 889–914
- Özsoy E, Latif MA, Beşiktepe S, Çetin N, Gregg N, Belokopytov V, Goryachkin Y, Diaconu V (1998). The Bosphorus Strait: exchange

- fluxes, currents and sea-level changes, In: Ivanov L and Oğuz T (editors), *Ecosystem Modeling as a Management Tool for the Black Sea*, NATO Science Series 2: Environmental Security 47, Kluwer Academic Publishers, Dordrecht, vol. 1, 367 pp + vol. 2, 385 pp
- Özsoy E, Di Iorio D, Gregg MC, Backhaus JO (2001) Mixing in the Bosphorus Strait and the Black Sea continental shelf: observations and a model of the dense water outflow. *J Mar Syst* 31:99–135
- Pacanowski R, Philander S (1981) Parameterization of vertical mixing in numerical-models of tropical oceans. *J Phys Oceanogr* 11(11):1443–1451
- Pinardi, N. (2009) *Misurare il mare. Luigi Ferdinando Marsili nell'Egeo e nel Bosforo 1679–1680*, Bononia University Press (collana *Grandi opere*), 83 pp
- Pinardi, N., Özsoy, E., Latif, M. A., Moroni, F., Grandi, A., Manzella, G., De Strobel, F. and V. Lyubartsev (2016) Measuring the sea: the first oceanographic cruise (1679–1680) and the roots of oceanography. (submitted for publication in *Deep Sea Res.*)
- Pratt LJ (2008) Critical conditions and composite Froude numbers for layered flow with transverse variations in velocity. *J Fluid Mech* 605:281–291
- Preller RH (1986) A numerical model study of the Alboran Sea gyre. *Prog Oceanogr* 16(3):113–146
- Rank D, Özsoy E, Salihoğlu İ (1998) Oxygen ^{18}O , deuterium and tritium in the Black Sea and the Sea of Marmara. *J Env Rad* 43: 231–245
- Roussenov V, Stanev E, Artale V, Pinardi N (1995) A seasonal model of the Mediterranean Sea general circulation. *J Geophys Res* 100(C7): 13515–13538
- Riha SA, Peliz A (2013) A two-layer primitive equation model of an idealized Strait of Gibraltar connected to an Eastern Basin. *Ocean Dyn* 36:615–631
- Sanchez-Garrido JC, Sannino G, Liberti L, Garcia Lafuente J, Pratt LJ (2011) Numerical modelling of three-dimensional stratified tidal flow over Camarinal Sill, Strait of Gibraltar. *J Geophys Res* 116: C12026. doi:10.1029/2011JC007093
- Sannino G, Carillo A, Artale V (2007) Three-layer view of transports and hydraulics in the Strait of Gibraltar: a three-dimensional model study. *J Geophys Res* 112:C03010. doi:10.1029/2006JC003717
- Sannino G, Carillo A, Pratt L (2009) Hydraulic criticality of the exchange flow through the Strait of Gibraltar. *J. Phys. Ocean.* 39(11):2779–2799. doi:10.1175/2009JPO4075.1
- Sannino, G., Garrido, J. C. S., Liberti, L. and L. Pratt (2014) Exchange flow through the Strait of Gibraltar as simulated by a s-coordinate hydrostatic model and a z-coordinate non hydrostatic model. In: G. Borzelli, M. Gacic, P. Lionello, P. Malanotte-Rizzoli (editors), *The Mediterranean Sea: Temporal Variability and Spatial Patterns*, American Geophysical Union, pp. 25–50. ISBN: 978–1–118–84734–3
- Sannino G, Carillo A, Pisacane G, Naranjo C (2015) On the relevance of tidal forcing in modelling the Mediterranean thermohaline circulation. *Prog Oceanogr* 134:304–329. doi:10.1016/j.pcean.2015.03.002
- Schroeder, K., Garcia-Lafuente, J., Josey, S. A., Artale, V., Nardelli, B. B., Carrillo, A., Gačić, M., Gasparini, G. P., Hermann, M., Lionello, P., Ludwig, W., Millot, C., Özsoy, E., Pisacane, G., Sánchez-Garrido, J. C., Sannino, G., Santoleri, R., Somot, S., Struglia, M., Stanev, E., Taupier-Letage, I., Tsimplis, M. N., Vargas-Yáñez, M., Zervakis, V., G. Zodiatis (2012). *Chapter 3: Circulation of the Mediterranean Sea and its Variability*, In: Lionello, P. (ed.), *The Climate of the Mediterranean Region—From the past to the future*, Elsevier, 592 p
- Soffientino B, Pilson M (2005) The Bosphorus Strait: a special place in the history of oceanography. *Oceanography* 18(2):17–23
- Sözer A (2013). *Numerical modeling of the Bosphorus exchange flow dynamics*, Ph.D. thesis, Institute of Marine Sciences, Middle East Technical University, Erdemli, Mersin, Turkey
- Sözer A, Özsoy E (2002) A three-dimensional model of bosphorus strait dynamics. The 2nd Meeting on the Physical Oceanography of Sea Straits, Villefranche-Sur-Mer, 15–19 April 2002, pp 207–210
- Sözer A, Özsoy E (2017). Modeling of the Bosphorus exchange flow dynamics, *Ocean Dynamics*, online, 23pp., DOI 10.1007/s10236-016-1026-z
- Spall M, Price JF (1998) Mesoscale variability in Denmark Strait: the PV outflow hypothesis. *J Phys Ocean* 28:1598–1623
- Staschuk N, Hutter K (2001) Modelling of water exchange through the Strait of the Dardanelles. *Cont Shelf Res* 21:1361–1382
- Stern M, Whitehead J, Hua B (1982) The intrusion of a density current along the coast of a rotating fluid. *J Fluid Mech* 123: 237–265
- Tolmazin D (1985) Changing coastal oceanography of the Black Sea, II. Mediterranean effluent. *Prog Oceanogr* 15:277–316
- Tonani M, Pinardi N, Dobricic S, Pujol I, Fratianni C (2008) A high-resolution free-surface model of the Mediterranean Sea. *Ocean Sci* 4(1):1–14
- Tuğrul S, Beşiktepe ŞT, Salihoğlu İ (2002) Nutrient exchange fluxes between the Aegean and Black Seas through the Marmara Sea. *Mediterranean Marine Sci* 3(1):33–42
- Tzali M, Sofianos S, Mantziafou A, Skliris N (2010) Modelling the impact of Black Sea water inflow on the North Aegean Sea hydrodynamics. *Ocean Dyn* 60:585–596
- Ünlüata Ü, Oğuz T, Latif MA, Özsoy E (1990) On the physical oceanography of the Turkish Straits. In: Pratt LJ (ed) *The physical oceanography of Sea Straits*. NATO/ASI Series, Kluwer, Dordrecht, pp 25–60